Nickel isotope fractionation during metal-silicate differentiation of planetesimals: Experimental petrology and *ab initio* calculations

J. Guignard [a,b,*], G. Quitté [a], M. Méheut [b], M.J. Toplis [a], F. Poitrasson [b]
D. Connetable [c], M. Roskosz [d]

[a] *IRAP, Université de Toulouse, CNRS, UPS, CNES, Toulouse, France*
[b] *GET, Université de Toulouse, CNRS, UPS, IRD, CNES, Toulouse, France*
[c] *CIRIMAT, CNRS, INP, ENSIACET, 4 allée Emile Monso, BP44362, 31030 Toulouse cedex 4, France*
[d] *IMPMC, CNRS, UMR 7590, Sorbonne Universités, Université Pierre et Marie Curie, Muséum National d'Histoire Naturelle, CP 52, 57 rue Cuvier, Paris F 75231, France*

Abstract

Metal silicate fractionation of nickel isotopes has been experimentally quantified at 1623 K, with oxygen fugacities varying from $10^{-8.2}$ to $10^{-9.9}$ atm and for run durations from 0.5 to 1 h. Both kinetic and equilibrium fractionations have been studied. A wire loop set up was used in which the metal reservoir is a pure nickel wire holding a silicate melt droplet of anorthite diopside eutectic composition. During the course of the experiment, diffusion of nickel from the wire to the silicate occurred. The timescale to reach chemical equilibrium was fO_2 dependent and decreased from 17 to 1 hour, as conditions became more reducing.

The isotopic composition of each reservoir was determined by Multicollector Inductively Coupled Plasma Mass Spectrometry (MC ICPMS) after Ni purification. The isotopic composition was found to be constant in the metallic wire, which therefore behaved as an infinite reservoir. On the contrary, strong kinetic fractionation was observed in the silicate melt (δNi down to $0.98\%o.amu^{-1}$ relative to the standard). Isotopic equilibrium was typically reached after 24 hours. For equilibrated samples at 1623 K, no metal silicate fractionation was observed within uncertainty (2SD), with $\Delta Ni_{Metal-Silicate} = 0.02 \pm 0.04\%o. amu^{-1}$.

Theoretical calculations of metal silicate isotope fractionation at equilibrium were also performed on different metal silicate systems. These calculations confirm (1) the absence of fractionation at high temperature and (2) a weak temperature dependence for Ni isotopic fractionation for the metal olivine and metal pyroxene pairs with the metal being slightly lighter isotopically.

Our experimental data were finally compared with natural samples. Some mesosiderites (stony iron meteorites) show a $\Delta Ni_{Metal-Silicate}$ close to experimental values at equilibrium, whereas others exhibit positive metal silicate fractionation that could reflect kinetic processes. Conversely, pallasites display a strong negative metal silicate fractionation. This most likely results from kinetic processes with Ni diffusion from the silicate to the metal phase due to a change of Ni partition coefficient during cooling. In this respect we note that in these pallasites, iron isotopes show metal silicate fractionation that is opposite direction to Ni, supporting the idea of kinetic isotope fractionation, associated with Fe Ni interdiffusion.

---

* Corresponding author at: IRAP, Université de Toulouse, CNRS, UPS, CNES, Toulouse, France.
E mail address: jeremy.guignard@irap.omp.eu (J. Guignard).

1. INTRODUCTION

Non traditional metal stable isotopes (e.g., Fe, Ni, Zn, Cu, Cr, Cd, Ga, Ge, Hg, Mo, U, W) have received growing attention over the past decade as they are powerful tools to trace (bio) geochemical processes ranging from alteration at the Earth's surface (e.g. McManus et al., 2002; Rouxel et al., 2003; Hohl et al., 2015; Noordmann et al., 2015; Wang et al., 2016; Baronas et al., 2018) to metal silicate dif ferentiation in planets and asteroids (e.g. Poitrasson et al., 2005, 2009; Georg et al., 2007; Schoenberg and von Blanckenburg, 2006; Luais, 2007; Hin et al., 2013; Bonnand et al., 2016; Kempl et al., 2016; Mahan et al., 2017; Liu et al., 2017; Bourdon et al., 2018).

Nickel (Ni) is the second most abundant element in the metallic cores of planetesimals and planets. It is thus an ele ment of major interest in the study of metal silicate differen tiation in the early solar system. Until recently, nickel isotopes have mainly been used for nucleosynthetic anoma lies applications (Quitté et al., 2006a; Regelous et al., 2008; Steele et al., 2011; Render et al., 2018) and in radiochronol ogy (Shukolyukov and Lugmair, 1993; Quitté et al., 2011; Tang and Dauphas, 2014) to date early events in the solar system based on the decay of ^{60}Fe to ^{60}Ni with a half life of 2.62 Ma (Rugel et al., 2009). Coupled with ^{26}Al, ^{60}Ni has also been used to quantify the available heat sources required for planetary melting, and thus to unravel thermal histories of meteorite parent bodies that accreted early in the protoplanetary disk (e.g. Tachibana and Huss, 2003; Telus et al., 2018). Mass dependent fractionation of nickel stable isotopes in meteorites and planetary bodies has received much less attention than other elements such as iron and silicon, mostly due to technical and analytical issues. Nonetheless, for roughly ten years, analytical devel opments have allowed the study of stable nickel isotopes across a wide range of scientific fields, from biological (Cameron et al., 2009), to oceanic (Fuji et al., 2011; Gueguen et al., 2016), environmental (Ratié et al., 2015a; 2016), planetary differentiation and cosmochemical pro cesses. First measured in the metallic phases (kamacite and/or taenite) of different types of meteorites (Quitté et al., 2006a; Cook et al., 2007; Dauphas, 2007; Moynier et al., 2007), nickel isotopic signatures exhibit large varia tions, from 0.05 to 0.30‰.amu^{-1}. Similarly, the Ni iso tope composition also varies within meteorite groups, e.g., among ordinary chondrites or iron meteorites types (Gall et al., 2017 and references therein). A fractionation is also observed as well in metal grains of CB/CH chondrites (Weyrauch et al., 2019). Last but not least, recent studies based on in situ measurements of nickel isotopes in silicate and metal phases in pallasites and mesosiderites show vari able metal silicate fractionation of nickel isotopes. In detail, pallasites exhibit negative metal silicate fractionation of nickel isotopes, from 0.106 ± 0.043 to 1.016 ± 0.080‰.amu^{-1}, whereas mesosiderites have positive metal silicate fractionation of nickel isotopes, spanning a narrower range, from 0.045 ± 0.009 to 0.170 ± 0.040‰. amu^{-1}. These differences in sign, range and absolute values possibly reveal various processes such as equilibrium, kinetic (diffusion and/or volatility) (Chernonozhkin et al.,

2016, 2017). Thus, Ni isotope fractionation seems a power ful tool to unravel important questions in planetology. However, nickel is strongly siderophile, which means that the Ni content in silicates is usually low. Nickel can be con sidered as a trace element in the main silicate minerals found in meteorites. For instance, nickel contents in mete oritic olivine is typically between 20 and 40 ppm in palla sites, but it can reach up to 0.25 wt% NiO in the olivines of more oxidized meteorites such as Rumurutiites (Petry et al., 1996). It is to note that in planetesimals, the main sil icate reservoir of Ni is olivine.

One of the key questions in planetology is whether the Ni isotope composition of the Bulk Silicate Earth (BSE) is chondritic or not. Based on various studies (Steele et al., 2011; Gueguen et al., 2013; Gall et al., 2017; Quitté et al., 2017; Klaver and Elliott, 2018), δNi values for the BSE span from 0.025‰.amu^{-1} to 0.115‰.amu^{-1} relative to chondrites. Hence it remains unclear whether the BSE and chondrites show the same isotopic composition within uncertainty or not, and nickel isotope data in planetary objects remain scarce. If this difference is confirmed, it could be explained by metal silicate differentiation. In par allel, the question can be tackled using an experimental approach. Contrary to iron, nickel is only present as Ni^{2+} in silicates. It can then help to decouple the various pro cesses responsible for isotope fractionation. According to Elardo and Shahar (2017), nickel is also an important ele ment to investigate, as it might be the ingredient controlling iron isotope fractionation during core formation. This remains a debated issue, however (Poitrasson et al., 2005, 2009; Chernonozhkin et al., 2016, 2017; Liu et al., 2017). Until now, a single experimental study exists and explores the isotope fractionation of Ni in a metal talc system (Lazar et al., 2012). Besides metal silicate differentiation, Ni isotopes can be fractionated by volatile depletion pro cesses in a way similar to Fe and Si, as suggested by Quitté et al. (2017) to explain the differences in isotope sig natures between the Earth, the Moon, Mars and Vesta. Indeed, nickel is a moderately volatile element that can eventually evaporate for long duration experiments at high temperature.

In the present study, high temperature (1623 K) experi ments have been performed under reducing conditions (fO$_2$ = 10$^{-8.2}$ and 10$^{-9.9}$ atm) to quantify kinetic and equi librium fractionations of nickel isotopes between a solid metal and a silicate melt under similar conditions. Accord ingly, most meteorites including pallasites, mesosiderites and primitive achondrites formed in a reducing environ ment (along the iron wüstite (IW) buffer to 5 log units below, i.e., from IW to IW 5). As stated above, Ni can only be present as Ni^0 or Ni^{2+} and its metal silicate partition coefficient depends on the oxygen fugacity. Hence, two dif ferent fO$_2$ conditions have been investigated in the frame of the present work. Additionally, first principles calculations were performed on different metal silicate mineral systems, namely Ni olivine and Ni diopside to determine theoretical equilibrium Ni isotope fractionation factors and their tem perature dependence. Both experimental and theoretical data are finally combined to interpret the variability of nickel isotopes signatures in meteorites.

2. METHODS

2.1. Experimental petrology

Experiments have been performed to approach metal silicate equilibrium in planetesimals. The metallic reservoir is a nickel wire 0.5 mm in diameter (Alfa Aesar, puratonic, 99.999%) and the silicate reservoir is a melt of anorthite diopside eutectic composition which corresponds to a good analogue of silicate composition in natural samples and that can cover a wide range of temperature under its liquid form. Pure Ni wire has been chosen instead of a Fe Ni alloy, more representative of a planetary metallic core, because Ni covers a wider range of fO_2 in its metallic form; its solubility in the silicate glass is therefore easier to control under reducing conditions. Besides, using pure Ni avoids interactions between different elements such as Fe Ni inter diffusion processes or competition between both. A large batch of the glass (≈ 50 g) was synthesized from reagent grade oxides (SiO_2; Alfa Aesar, 99.8% and Al_2O_3; Acros Organics, 99+%, extra pure) or carbonates ($CaCO_3$; Acros Organics, 99+% and $4(MgCO_3) \cdot Mg(OH)_2 \cdot 5(H_2O)$; Acros Organics, containing 40.39 wt% MgO). The starting mixture was first fired to 1073 1273 K for several hours to ensure complete dehydration and decarbonation. The mixture was then melted in air in a platinum crucible at 1723 K for 2 hours, quenched and finely crushed in an alumina mortar. These steps were repeated twice to obtain a well homogenized glass as demonstrated by the multiple (≈ 100) electron microprobe analyses of its composition (Table 1).

Time series experiments were performed using the wire loop set up. Glass droplets of approximately 30 mg were prepared and suspended on a Ni wire loop (~ 25 mg). In this setup, at high temperature, nickel diffuses from the wire to the silicate melt where its concentration rapidly reaches chemical equilibrium. For each experiment, 5 samples were loaded simultaneously in the furnace and quenched in air at different times, thereby allowing to quantify kinetic effects. All experiments were performed at a single temperature (1623 ± 1 K). Two different oxygen fugacities ($10^{-8.2}$ and $10^{-9.9}$ atm; i.e., 2 and 3.7 log units below the Ni NiO buffer) were used, fixed by $CO:CO_2$ gas mixture. These conditions of temperatures and fO_2 have been chosen to mimic conditions of metal silicate differentiation in natural objects. Run durations ranged from 30 minutes to 7 days (Table 2). Replicate experiments were carried out in order to confirm the reproducibility of the experimental conditions and

results. In details, experiments at 24 hours were at least duplicated for both types of experiments.

2.2. Nickel separation and analysis

After experiments, the metallic wire and the silicate glass droplet were mechanically separated under a binocular microscope. Each part was then digested on a hotplate at 120 130 °C for at least 3 days in a mixture of HCl, HF and HNO_3 with volume ratios 2:1:1 and 1:1:0.05, for metal and silicate, respectively, and in a total volume of 4 ml. After digestion, samples were dried and then taken up in 2 ml of 6 N HCl twice to convert fluorides into chlorides. A small aliquot of 5 % in volume was then saved for concentration analysis (using ICP OES and/or ICP MS) and the remaining solution was dried down again, ready for nickel separation.

The latter consists of four steps and follows the method developed by Quitté and Oberli (2006b). The main difference in the chemical separation between metal and silicate is that the dimethylglyoxime (DMG) step (see below) is not used for Ni wires. Briefly, the samples were re dissolved in 2 ml 9 N HCl and loaded on a AG1 X8 anion exchange resin. As nickel elutes immediately, it was directly collected in the load fraction. Elution was completed with additional 4 ml of 9 N HCl. After evaporation, the sample was taken up in 2 ml 2 N HCl and loaded once more on the same resin. Nickel elution was again completed with 4 ml of HCl 2 N. These two steps allowed efficient separation of iron and zinc, two elements that have isobaric interferences with nickel at masses 58 and 64 respectively. The dry samples were then dissolved in 5 mL of 1 N HCl and 1 ml of 1 N ammonium citrate and the pH was adjusted to 8 9 with a few drops of concentrated ammonia. The samples were subsequently loaded on a Ni specific resin containing DMG that complexes Ni and lets most of all other elements flow through the resin. Only few elements form chelates with DMG: Ni, Co, Cu, Pd and Pt. Copper and Cu were separated during the first step using AG1 X8 resin, hence they are not present in the Ni cut anymore. Contrary to Ni, palladium only reacts with DMG in acid solution, and platinum and Pd are anyway removed later during the separation procedure (see below). Elution of this Ni DMG organic complex was achieved by adding 12 ml of 3 N HNO_3. In order to break the Ni DMG complex, a few drops of $HClO_4$ were added to the solution before it was evaporated to dryness. To destroy organic matter originating from the resin and residual DMG in the case of

Table 1
Starting composition of the silicate glass.

	Expected starting composition (wt%)	[a]Measured starting composition (wt%)
SiO_2	50.33	50.52(35)[b]
CaO	23.49	22.95(31)[b]
Al_2O_3	15.39	15.22(25)[b]
MgO	10.79	11.30(19)[b]

[a] Average value of measurements made on 100 electron microprobe points.
[b] Number in parentheses indicate two standard deviation on the last two digits.

Table 2
Experimental data.

Sample	Temperature (K)	Log fO_2 (atm)	Time (hours)	Concentration (10^3ppm)[a]	[b]δNi_M (a.m.u^{-1})	[b]δNi_S (a.m.u^{-1})	ΔNi_{M-S}	Replicates[c]
Ni_{wire}	298	Air	0	10^3	0.25 (06)			7
Ni_{wire}+(An:Di)$_{melt}$	1623	8.2	0.5	2.64 (49)[d]	0.25 (08)	0.77 (08)	0.52 (11)	6/4
Ni_{wire}+(An:Di)$_{melt}$	1623	8.2	1	3.74 (77)[d]	0.27 (03)	0.80 (11)	0.53 (11)	5/5
Ni_{wire}+(An:Di)$_{melt}$	1623	8.2	2	4.88 (60)[d]	0.26 (03)	0.98 (05)	0.72 (06)	3/4
Ni_{wire}+(An:Di)$_{melt}$	1623	8.2	3	5.68 (98)[d]	0.26 (09)	0.42 (04)	0.16 (10)	5/3
Ni_{wire}+(An:Di)$_{melt}$	1623	8.2	5	6.01 (43)[d]	0.23 (05)	0.40 (11)	0.18 (12)	4/5
Ni_{wire}+(An:Di)$_{melt}$	1623	8.2	10.6	6.97 (41)[d]	0.28 (06)	0.38 (04)	0.10 (07)	3/4
Ni_{wire}+(An:Di)$_{melt}$	1623	8.2	17.9	8.81 (16)[d]	0.27 (02)	0.39 (04)	0.13 (05)	3/4
Ni_{wire}+(An:Di)$_{melt}$	1623	8.2	24	9.13 (17)[d]	0.21 (05)	0.21 (06)	0.00 (07)	4/5
Ni_{wire}+(An:Di)$_{melt}$	1623	8.2	24	8.95 (11)[d]	0.26 (02)	0.33 (06)	0.07 (07)	3/4
Ni_{wire}+(An:Di)$_{melt}$	1623	8.2	48	9.20 (38)[d]	0.27 (05)	0.30 (06)	0.03 (08)	3/4
Ni_{wire}+(An:Di)$_{melt}$	1623	8.2	168	8.90 (15)[d]	0.13 (01)	0.14 (01)	0.01 (01)	3/3
Ni_{wire}+(An:Di)$_{melt}$	1623	9.9	0.5	1.01 (02)[e]	0.25 (02)	0.74 (04)	0.50 (05)	3/3
Ni_{wire}+(An:Di)$_{melt}$	1623	9.9	1	1.14 (01)[e]	0.26 (02)	0.62 (03)	0.36 (03)	3/5
Ni_{wire}+(An:Di)$_{melt}$	1623	9.9	2.8	1.31 (01)[e]	0.24 (02)	0.39 (03)	0.15 (04	3/4
Ni_{wire}+(An:Di)$_{melt}$	1623	9.9	24	1.35 (01)[e]	0.24 (03)	0.27 (07)	0.03 (07)	3/4
Ni_{wire}+(An:Di)$_{melt}$	1623	9.9	24	1.34 (01)[e]	0.24 (02)	0.27 (01)	0.03 (03)	3/4
Processed Ni std	298	Air		0.0003	0.02 (02)			3
Glass + Ni std	298	Air		0.0003	0.01 (02)			3

[a] Numbers in parentheses represent 2SD on the last two digits, determined from at least three replicates.
[b] M = Metal, S = silicate melt.
[c] Metal/silicate.
[d] Measured by ICP OES.
[e] Measured by ICP MS.

Ni rich samples, the dried samples were then dissolved twice in a 30% H_2O_2 + 16 N HNO_3 (1 ml + 1 ml) mixture and evaporated again to dryness. Finally, the samples were taken up in 0.2 ml H_2O and loaded onto a AG50W X8 cationic resin for a final purification step. The main goal of this third step using small columns is to remove organic matter, as well as Pt and Pd if any. Matrix elements were washed out with 2.5 mL of 0.2 N HCl and nickel was eluted with 0.5 ml of 3 N HCl and evaporated to dryness. The yield of this procedure was 95 ± 3%. The small loss of Ni occurred when using dimethylglyoxime (DMG) on the second column and induced no Ni isotope fractionation as witnessed by the isotope composition of the processed standard, similar to that of the unprocessed isotope standard.

Nickel isotope measurements were performed using a combination of the standard sample bracketing technique and Cu doping using a Neptune MC ICPMS (ThermoFischer Scientific) in "medium resolution mode", i.e., a resolving power $M/\Delta M \approx 7000$ (5 95% peak edge definition) at the Observatoire Midi Pyrénées, Toulouse. A double spike approach was not used for Ni isotope analyses in this study to avoid clean laboratory and our instrument contamination. Besides this study, we also conduct in Toulouse the measurement of mass independent variations of Ni isotopes in cosmochemical samples, which are particularly sensitive to small uncertainties in ^{61}Ni, ^{62}Ni and ^{64}Ni, especially when looking at nucleosynthetic anomalies. The Cu doping method adopted in this study has a reproducibility comparable to that attained using a double spike approach. All

nickel isotopes (58, 60, 61, 62, 64) were measured simultaneously as well as ^{57}Fe and ^{66}Zn in order to correct for isobaric interferences of ^{58}Fe on ^{58}Ni and ^{64}Zn on ^{64}Ni. These corrections are efficient if the Fe/Ni and Zn/Ni ratios are lower than 0.1 and 10^{-3} respectively (Quitté and Oberli, 2006b). This is always the case for Fe/Ni ratios, but more difficult to control for Zn/Ni due to external Zn contamination, hampering the systematic use of ^{64}Ni.

After nickel separation and purification, samples were dissolved in 0.1 N HCl and their Ni concentration was adjusted to match within 10 % the concentration of the bracketing standard (an Aldrich standard solution). Moreover, in order to correct for the instrumental mass bias, copper (Cu) was used as an internal standard and an exponential law was considered for the calculation. Copper was added both to samples and standards, typically to half the concentration of nickel. Hence, ^{63}Cu and ^{65}Cu were measured in a second cycle during the run in dynamic mode (one cycle for Ni, Fe and Zn isotopes, the other for Cu). ^{60}Ni is a radiogenic isotope whose abundance may vary in meteorites due to in situ decay of ^{60}Fe. We therefore prefer to avoid ^{60}Ni when reporting mass dependent isotope fractionation in meteorites or in experiments when the experimental data are dedicated to interpret results obtained in natural samples. Besides, once evidence is provided that the observed fractionation follows a mass dependent law (see Fig. 2), the reported $\delta^{i/j}$Ni ratio does not matter (i and j can be any isotope of Ni). Reporting the isotope fractionation per atomic mass unit (a.m.u.) should allow a direct and easy comparison with literature data.

This notation has already been used by different authors for, e.g., Cu, Zn, Ca, Ni.

All nickel isotopic ratios are reported relative to the Ni Aldrich standard corrected for mass bias using the internal standard, and expressed according to the following equation:

$$\delta Ni\left(\text{‰}.amu^{-1}\right) = \left(\frac{(^iNi/^jNi)_{sample-Cu\,corr}}{(^iNi/^jNi)_{std-Cu\,corr}} - 1\right) \times \frac{1000}{(i-j)}$$

where $(^iNi/^jNi)_{sample-Cu\,corr}$ is the measured $^iNi/^jNi$ ratio in the sample corrected for the mass bias using copper and $(^iNi/^jNi)_{std-Cu\,corr}$ is the average of the $^iNi/^jNi$ ratio of the standards that bracket the sample in the analytical sequence, corrected from mass bias using copper. Measurements of the Aldrich standard solution relative to the certified SRM986 isotope standard confirmed that both have the same isotopic composition ($\delta Ni = -0.05 \pm 0.06$‰. amu^{-1}). A standard processed through the whole separation procedure shows an isotopic composition of -0.02 ± 0.02‰.amu^{-1} demonstrating that our nickel purification procedure does not fractionate its isotopes. The external reproducibility (2 SD) achieved on standard replicates over a year, i.e., ≈300 measurements, is 0.04‰.amu^{-1} and 0.07‰.amu^{-1} for $\delta(^{62}Ni/^{58}Ni)$ and $\delta(^{64}Ni/^{58}Ni)$, respectively. Similar reproducibility is found on the nickel wire ($\delta Ni_{starting\,metal} = -0.25 \pm 0.06$‰.amu^{-1}, n = 7 replicates). To check accuracy of the isotope measurements, a glass droplet comparable to those used for the experiments, but doped with our Aldrich Ni standard, was also processed: it yields a δNi of -0.01 ± 0.02‰.amu^{-1}, undistinguishable from the matrix free processed and unprocessed standards. Hence, isotope analyses are not hampered by matrix effects. We also note that there is no evidence of correlation between the reproducibility and odd / even isotope pairs, indicating no significant mass independent fractionation effect, if any. The external reproducibility on the samples is calculated on at least three replicate measurements (Table 2). Finally, the nickel isotope fractionation between metal and silicate melt (ΔNi_{M-S} in amu^{-1}) is expressed as:

$$\Delta Ni_{M-S} = \delta Ni_M - \delta Ni_S, \tag{2}$$

with δNi_M the nickel isotope composition in the metal (in amu^{-1}) and δNi_S the isotope composition of the silicate melt (in amu^{-1}).

2.3. ab-initio calculation

A theoretical approach was also used to estimate the ΔNi_{M-S} at equilibrium for different metal silicate systems with the aim to compare them with the experimental data, to refine the interpretation of the latter and to extrapolate to lower temperature conditions.

Equilibrium fractionation properties of condensed phases are expressed theoretically by their β factors, which are related to the change in free energy associated with isotopic substitution in a particular phase. The connection between the Δ values and the β factors is expressed via the isotopic fractionation between phases A and B:

$$\Delta Ni_{A-B} = 1000 \ln \beta Ni_A - 1000 \ln \beta Ni_B, \tag{3}$$

where $\ln \beta Ni_{A(B)}$ are the so called β factors of Ni isotopes in phase A (respectively B).

β factors of metal and silicate phases have then been computed from their phonon frequencies based on the general theory (see e.g. Meheut et al., 2007).

For the metal (pure Ni, fcc structure), the phonon frequencies were computed from first principles using density functional theory (DFT) (Hohenberg and Kohn, 1964; Kohn and Sham, 1965). The calculation was based on the exchange correlation functional of Perdew, Burk and Ernzerhof (PBE) (Perdew et al., 1996), a plane wave basis set, and atomic pseudopotentials as implemented in the Quantum Espresso package (Giannozzi et al., 2009). Pseudopotentials used for Si, O, H are described in Méheut et al. (2007). The pseudopotential used for Ni comes from the GBRV (Garrity, Benneth, Rabe, Vanderbilt) pseudopotential library version 1.4 (Garrity et al., 2014), verified within the SSSP (Standard Solid State Pseudopotentials) effort (Lejaeghere et al., 2016).

For the silicate phases, the calculation may be more difficult. Indeed, insulators containing transition elements appear sometimes challenging to model, due to the failure of classical DFT methods to model strongly correlated electronic systems (Cococcioni et al., 2005). In this case, a + U correction might be necessary for the calculation to correctly reproduce the insulating behavior of these systems (Cococcioni et al., 2005). However, we note that the insulating materials considered in this study (Ni olivine and Ni diopside) were found to be insulators even without a +U correction, suggesting that this latter correction is not necessary in the calculations (Zbiri et al., 2008). Therefore, in the present study calculations were performed without the +U correction. Finally, these different phases show complex magnetic orders (Hagemann et al., 2000; Durand et al., 1996). In order to quantify the effect of this order, different tests have been performed on Ni olivine structure (see discussion in the Appendix). Such tests show that the type of magnetic order has a negligible effect on the calculated fractionation properties (Fig. 1 of the Appendix).

Following these considerations, in the rest of this study, the magnetic structure considered for Ni olivine is the one referred to as configuration 1 by Cococcioni et al. (2005) (who studied Fe olivine), as it is slightly better in reproducing experimental structure (see Appendix). For Ni metal and Ni diopside, a ferromagnetic structure was considered. The structural parameters of Ni metal were found to be virtually indistinguishable from experimental ones, whereas those of silicates were found to be 1 2% larger than the experimental ones, which is typical of this type of method (Table 1 of Appendix).

Electronic wave functions were expanded in plane waves up to an energy cutoff $\varepsilon_{cut} = 60$Ry for the metal and $\varepsilon_{cut} = 80$Ry for the silicates, and the charge density cut off set to $8\varepsilon_{cut}$. The electronic structure integration was performed by sampling the first Brillouin zone with a $20 \times 20 \times 20$ k points grid for the Ni metal, a $2 \times 2 \times 2$ k point grid for Ni_2SiO_4 and a $2 \times 3 \times 2$ k point grid for $CaNiSi_2O_6$.

The dynamical matrices were computed using the linear response of Baroni et al. (2001), with the PWSCF package

(Giannozzi et al., 2009), exactly (within DFT) on different grids of q vectors ($8 \times 8 \times 8$ for Ni metal, $2 \times 2 \times 2$ for Ni_2SiO_4, $2 \times 3 \times 2$ for $CaNiSi_2O_6$). The phonon frequencies were then obtained in any point of reciprocal space using the standard Fourier interpolation technique. For silicate materials the vibrational partition function was converged with a $6 \times 6 \times 6$ interpolation grid, while for metal a $20 \times 20 \times 20$ grid was used.

3. RESULTS

3.1. Concentrations

Concentrations of Ni have only been measured in bulk silicate glasses after sample digestion, using ICP OES at IPGP Paris, or ICP MS at the OMP, Toulouse, depending on instrument availability (Table 2 & Fig. 1). Nickel concentration in the wire has not been measured since it is made of ultrapure Ni. For experiments performed at $fO_2 = 10^{-8.2}$ atm (Fig. 1a), the Ni concentration increases with time, from 2600 ppm after 30 minutes of heat treatment at 1623 K to ≈ 9000 ppm after 17.9 hours. For longer durations, concentration remains constant at least up to 48 hours suggesting that chemical equilibrium is reached. For experiments performed under more reducing conditions, i.e. $fO_2 = 10^{-9.9}$ atm (Fig. 1b), the Ni concentration increases from 1000 ppm after 0.5 hours of heat treatment to 1300 ppm after 2.8 hours; For longer times up to 24 hours this concentration remains stable. Thus, chemical equilibrium is reached ≈ 6 times faster under these more reducing conditions. These results are in very good agreement with previous studies on the solubility of Ni in a silicate melt of similar composition at various temperatures and oxygen fugacity conditions (see Eq. (3) in Dingwell et al., 1994).

3.2. Isotope fractionation

For each experiment, the isotopic compositions of the metal wire and of the silicate melt have been determined and are presented in Table 2, Figs. 2 and 3. The starting metal (Ni_{wire}) has a composition of $\delta Ni_{wire} = 0.25 \pm 0.06\permil.amu^{-1}$, measured on 7 replicates. In all samples, Ni in both metal and silicate is isotopically lighter compared to the bracketing standards; their δNi values ranging from 0.28 to 0.13$\permil.amu^{-1}$ (for longest experiment, see explanation below) for the metal and from 0.98 to 0.14$\permil.amu^{-1}$ for the silicate melt (Table 2). In a three isotope diagram $\delta^{61/58}Ni$ vs $\delta^{62/58}Ni$, Ni data plot on a mass dependent fractionation line, with a slope of 0.967 ± 0.065, considering x and y error bars on each point. Considering different datasets for each phase during kinetic or equilibrium experiments show that slopes and error bars that are in the same range of the whole dataset (Fig. 2). Theoretical equilibrium (β_{eq}) and kinetic (β_{kin}) exponents have also been calculated, and reported in a.m.u^{-1}, according to the following equations modified from Young et al. (2002) (Fig. 2):

$$\beta_{eq} = \left(\frac{(1/m_{58} - 1/m_{62})}{(1/m_{58} - 1/m_{61})} \right) \times \left(\frac{m_{58} - m_{61}}{m_{58} - m_{62}} \right) \tag{4}$$
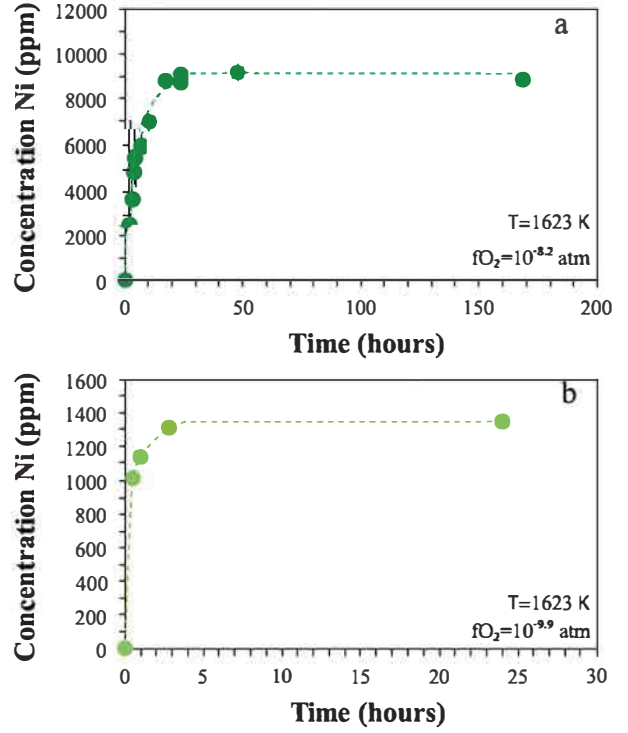

Fig. 1. Evolution of Ni concentration (in ppm) in the silicate melt with time and for the two studied oxygen fugacity conditions, (a) $10^{-8.2}$ atm and (b) $10^{-9.9}$ atm. Chemical equilibrium is reached after 17 hours for the most oxidizing conditions (a) and after only 0.5 hour in the other case (b). In both cases, concentrations measured at equilibrium are in very good agreement with the solubility of Ni in silicate melt with similar composition, calculated from the solubility law after Dingwell et al. (1994).

and,

$$\beta_{kin} = \left(\frac{ln(m_{58}/m_{62})}{ln(m_{58}/m_{61})} \right) \times \left(\frac{m_{58} - m_{61}}{m_{58} - m_{62}} \right) \tag{5}$$

where m is the mass of a given isotope. β_{eq} and β_{kin} are found to be very close, respectively 0.992 and 0.984; therefore, on such narrow range of isotopic composition, they are barely distinguishable (Fig. 2). Finally, based on this 3 isotopes plot on a narrow range of composition, the current analytical precision does not permit to discuss the origin (kinetic and/or equilibrium) of the observed isotope variations (Fig. 2, different slopes for the different subsets).

The evolution of isotopic compositions (δNi) of each reservoir (respectively δNi_M and δNi_S for metal and silicate) with time and for two different oxygen fugacity conditions is shown in Fig. 3a b. For the metal reservoir, from 0 to 48 hours of heat treatment and whatever the oxygen fugacity conditions, δNi_M remains constant within uncertainties ($\delta Ni_M = 0.25 \pm 0.05\permil.amu^{-1}$), and indistinguishable from the starting metal ($\delta Ni_{starting\ metal} = 0.25 \pm 0.06\permil.amu^{-1}$, n = 7 replicates) (Table 2, Fig. 3a b). For the silicate fractions, δNi_S is strongly time dependent and becomes heavier with time during the first 24 hours, starting from values at 0.77 $\pm$ 0.08$\permil.amu^{-1}$ after 30 minutes, decreasing to 0.98 $\pm$ 0.05$\permil.amu^{-1}$ after 2 hours at $fO_2 = 10^{-8.2}$

atm to 0.21 ± 0.06‰.amu^{-1} after 24 hours. For longer times, in the range 24 to 48 hours, δNi_S does not evolve suggesting that isotopic equilibrium is reached. The same trend is found for experiments at lower $fO_2 = 10^{-9.9}$ atm. for 24 hours. Therefore, an equilibrium isotope fractionation factor of ΔNi_{M-S} of 0.02 ± 0.04‰.amu^{-1} between metal and silicate has been inferred from different 24 h and 48 h experiments (experiments at 1623 K and $fO_2 = 10^{-8.2}$ atm for 24 h and 48 h performed twice). Within uncertainty, there is thus no metal silicate melt fractionation of Ni isotopes at equilibrium under these conditions.

However, for the longest experimental runs (i.e., t = 168 hours), both metal and silicate melt isotope compositions evolve towards slightly heavier compositions (δNi_M = 0.13 ± 0.01‰.amu^{-1} and δNi_S = 0.14 ± 0.01‰.amu^{-1} respectively). This indicates that light isotopes are partially lost from the overall metal + silicate system, which may be interpreted as the result of a small amount of Ni loss by volatility in the open experimental system, as already observed in the case of iron isotopes in similar systems (Prissel et al., 2018). Moreover, according to Wang et al. (1994) and Tsuchiyama and Fujimoto (1995), the evaporative loss of iron preferentially occurs in metal that in the silicate. However, ΔNi_{M-S} remains the same, within uncertainties, as determined for 24 h or 48 h experiments, i.e., $\Delta Ni_{M-S} = 0.01 \pm 0.01$‰.amu^{-1}, suggesting that the timescale for isotopic re equilibration of the sample is faster than evaporative loss of nickel.

3.3. Theoretical metal-silicate equilibrium fractionation of nickel isotopes

The evolution with temperature (for T > 400 K) of reduced partition function ratios (also called β factors of $^{62}Ni/^{58}Ni$) of metal and silicate is illustrated in Fig. 4. For all phases, β factors decrease linearly with increasing temperature (i.e. decreasing $1/T^2$). Metal ($Ni_\bullet$ or $Fe_\bullet$) exhibits lower β factors compared to silicate minerals (where Ni is present as Ni^{2+}), consistently with the rule of thumb relating fractionation and redox state (Schauble 2004, see also discussion in the Appendix sec. 1.2). For the latter, Ni rich olivine (Ni_2SiO_4, orthorhombic structure) and Ni rich pyroxene ($CaNiSi_2O_6$, monoclinic structure) are barely distinguishable at any temperature suggesting that nickel isotopes have similar properties regardless of the structure and composition of these anhydrous silicates.

From the calculation of these β factors, equilibrium metal silicate fractionations (ΔNi_{M-S}) have been determined as a function of temperature and reported in a.m.u^{-1} (Fig. 5). Best fits to the calculations for metal olivine and metal pyroxene systems are described by the equations:
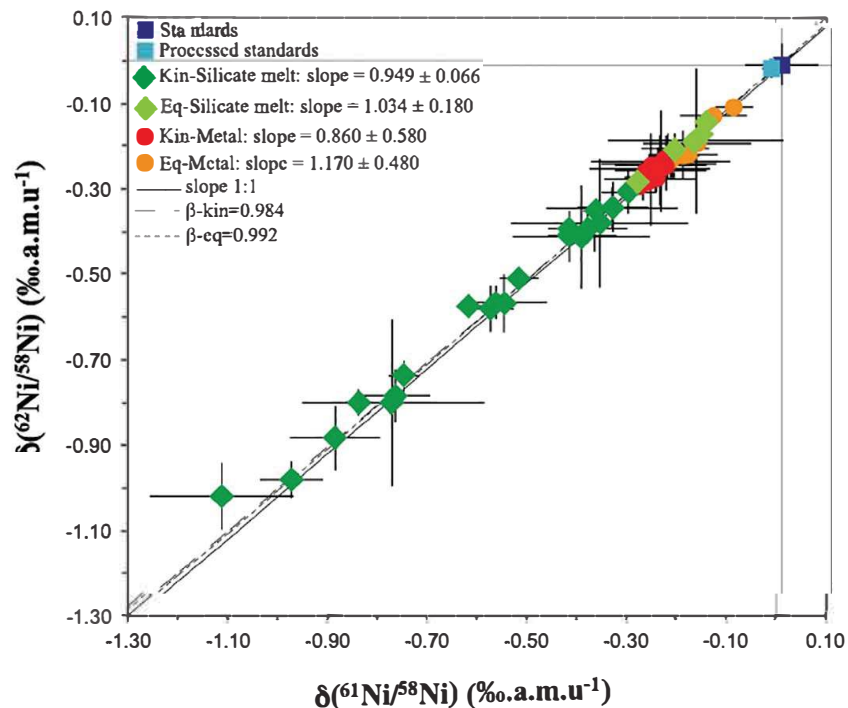

Fig. 2. Three isotope diagram. Data follow the trend expected for mass dependent fractionation (i.e., a line with a slope equal to 1 black line). Long and short dashed lines represent kinetic (β_{kin} = 0.984) and equilibrium (β_{eq} = 0.992) slopes calculated with the formulas of Young et al. (2002) and are barely distinguishable on this range of values. Dataset for each phase has been split between kinetic and equilibrium experiments. Slopes and errors (2SD) have been determined for each sub dataset considering error bars on both *x* and *y*. In any case, it is impossible to clearly distinguish between kinetic and equilibrium effects. Plotted errors are 2SD. Dark green circles = kinetic silicate melt; Light green circles = equilibrium silicate melt; red circles = kinetic Ni wire, orange circles = equilibrium Ni wire; dark blue circles = bracketing standards, light blue circle = standards processed on columns.
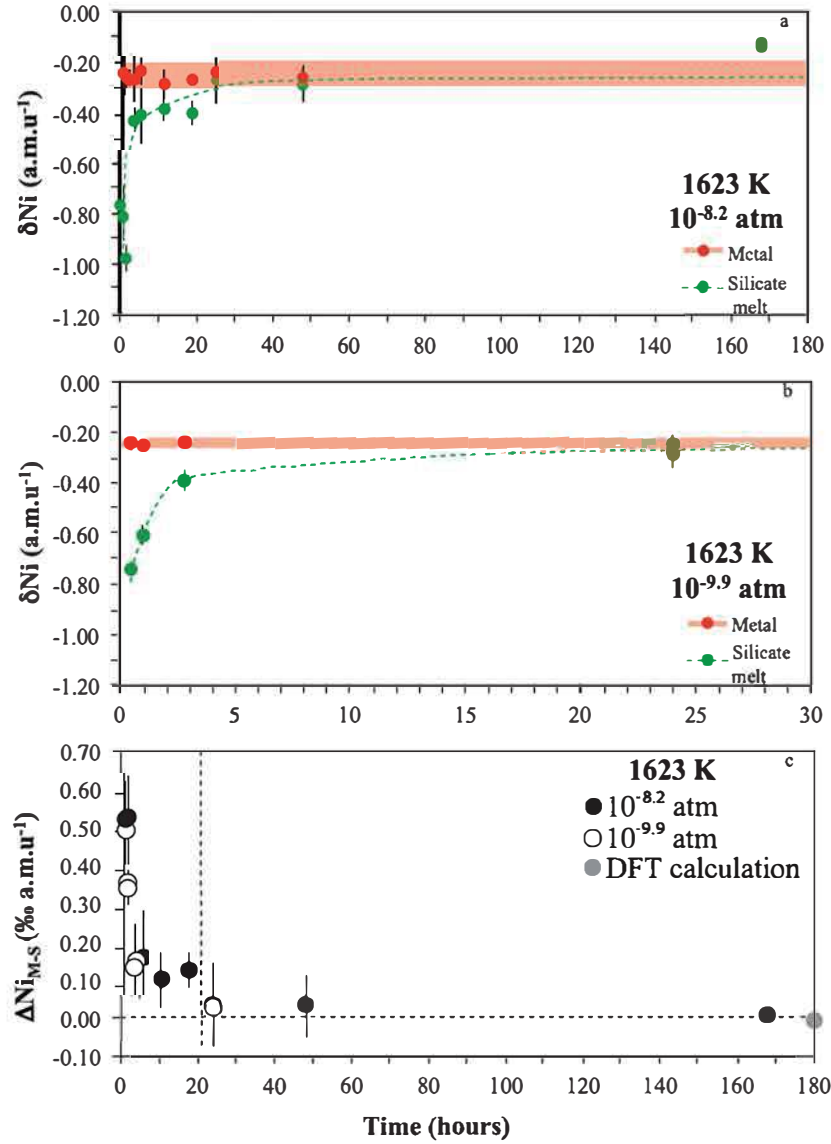
Fig. 3. Nickel isotope compositions (δNi in per mil per amu $^{-1}$) of metal and silicate fractions. (a) At 1623 K and $fO_2 = 10^{-8.2}$ atm and (b) at 1623 K and $fO_2 = 10^{-9.9}$ atm. Errors bars are 2SD on n replicates (see Table 2). Note that isotopic equilibrium is reached between 17 and 24 hours, thus later than chemical equilibrium. Nickel isotope compositions of metal fractions are constant over time suggesting an infinite reservoir behavior, whereas nickel isotope compositions of silicate melts are strongly variable. Measured equilibrium fractionation is in very good agreement with theoretical calculations (c, grey circle).

$$\Delta Ni_{metal-olivine} = 1.575 \times \frac{10^4}{T^2} + 2.580 \times \left(\frac{10^4}{T^2}\right)^2, \qquad (6)$$

$$\Delta Ni_{metal-pyroxene} = 1.440 \times \frac{10^4}{T^2} + 2.605 \times \left(\frac{10^4}{T^2}\right)^2, \qquad (7)$$

Metal silicate fractionations are negative and decrease linearly with increasing temperature. The temperature dependence is weak for metal olivine and metal pyroxene, leading to ΔNi_{M-S} variations from $-0.09‰.amu^{-1}$ at 400 K to $-0.005‰.amu^{-1}$ at 1623 K (i.e. the temperature of our experiments) for metal olivine, and $-0.08‰.amu^{-1}$ to $-0.006‰.amu^{-1}$ for metal pyroxene. A Nuclear Field

Shield Effect (NFSE) has also been taken into account using ground state energy of Ni^0 (typically in metal) and Ni^{2+} (typically in silicate) of the different nickel isotopes (Fuji et al., 2011 and Fig. 5). The NFSE by itself produced a small positive metal silicate fractionation, ranging from $0.02‰.amu^{-1}$ at 400 K to $0.006‰.amu^{-1}$ at 1623 K. Adding this NFSE to our calculated mass dependent fractionation (MDF) shifts the metal silicate fractionation to slightly higher values (Fig. 5), especially at lower temperature because NFSE is $1/T$ dependent whereas MDF (Mass Dependent Fractionation) is a function of $1/T^2$ (Fig. 5). Finally, considering the MDF alone or adding the NFSE yields the same conclusion when comparing the results of

the calculations with our experimental data at isotopic equilibrium ($\Delta Ni_{M-S} = 0.02 \pm 0.04‰.amu^{-1}$). Therefore, within uncertainties, both our experimental and theoretical approaches agree with each other (Figs. 3c and 5).

4. DISCUSSION

4.1. Equilibrium isotope fractionation under relevant conditions of metal-silicate differentiation

Experiments and *ab initio* calculations from this study show that under conditions relevant to metal silicate differentiation in planetesimals, (i.e. high temperature 1623 K, and negligible pressure effects), nickel isotope fractionation at equilibrium is negligible, with ΔNi_{M-S} values of 0.02 $\pm$ 0.04‰.amu^{-1} in our experiments and 0.005‰.amu^{-1} inferred from *ab initio* calculations (Table 2, Figs. 3c and 5). Besides, in experiments, attainment of isotopic equilibrium is not fO$_2$ dependent (Fig. 3) whereas chemical equilibrium is (Fig. 1). This fO$_2$ dependence of chemical equilibrium is due to the variations of metal/silicate partitioning coefficient which is higher at more reducing conditions, leading to faster saturation of silicate at lower fO$_2$. On the other hand, attainment of isotopic equilibrium is not dependent on the partition coefficient; therefore, isotope diffusion continues after chemical equilibrium is reached as long as temperature, i.e., diffusion coefficient, is high enough.

To the best of our knowledge, before the current work, a single experimental study has been published on Ni isotope fractionation between metal and silicate (Lazar et al., 2012). In that study, isotope fractionation between a synthetic Ni talc (isotopically spiked) and Ni metal (natural isotopic abundances) was estimated using the three isotope method, in a piston cylinder apparatus at different temperatures (from 773 to 1173 K), relatively low pressure ($\approx$ 1 GPa) and oxygen fugacity buffered around the Ni/NiO equilibrium. Under these conditions, $\Delta^{62}Ni_{metal-talc}$ (i.e., $\Delta(^{62}Ni/^{58}Ni)_{M-S}$) was found to be systematically positive and to decrease with increasing temperature from 0.44 $\pm$ 0.05‰ to 0.18 $\pm$ 0.03‰ ($\Delta T = 400$ K). Considering the metal talc system, Lazar et al. (2012) demonstrated that the fractionation could be calculated as $\Delta^{62}Ni_{metal-talc} = 0.25(\pm0.02) \times \frac{10^6}{T^2}$. Extrapolation using this equation shows that the fractionation factor at core mantle boundary conditions is negligible: ΔNi metal talc is 0.01‰.amu^{-1} at 2500 K and varies between 0.025 and 0.045‰.amu^{-1} for
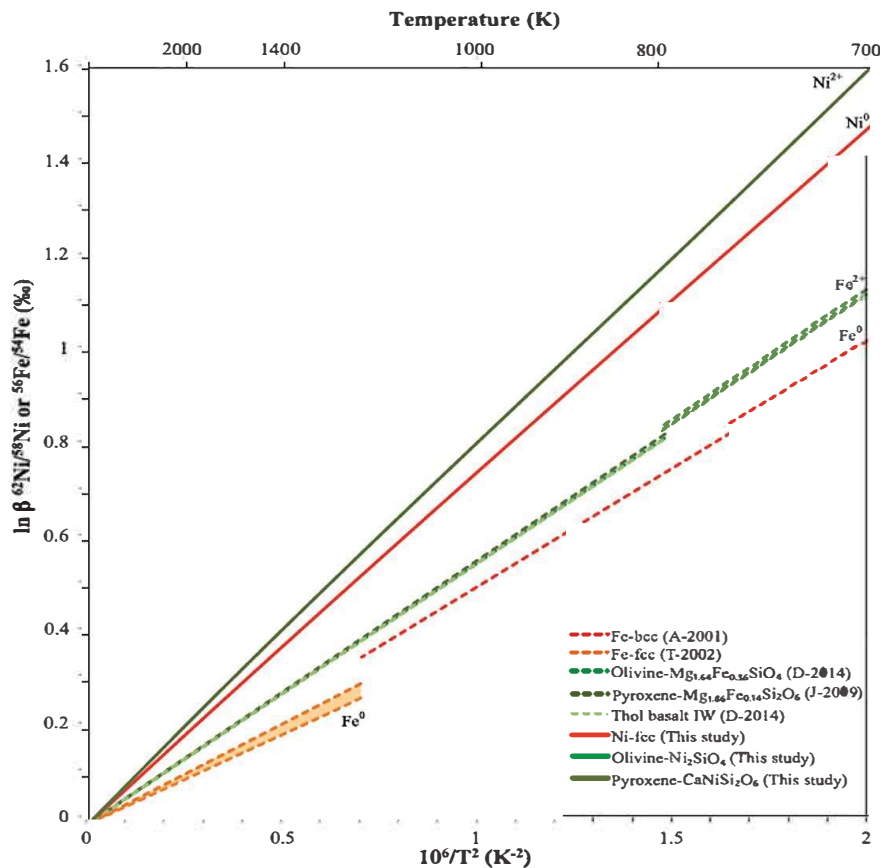

Fig. 4. (a) Reduced isotopic partition function ratios (β factors) of $^{62/58}$Ni in different mineral species relevant for planetesimals (+talc) as a function of temperature, calculated by the DFT method. For comparison, β factors of $^{56/54}$Fe determined by NRIXS (Nuclear Resonant Inelastic X ray Scattering) are shown for similar species (A 2001 = Alp et al., 2001; T 2002 = Tsunoda et al., 2002; J 2009 = Jackson et al., 2009; D 2014 = Dauphas et al., 2014). $^{62/58}$Ni β factors increase with oxidation state of Ni, from Ni^0 to Ni^{2+} as well as for $^{57/54}$Fe β factors. Besides, a similar behavior can be observed for olivine and pyroxene containing iron or nickel (Ni$_2$SiO$_4$ and CaNiSi$_2$O$_6$ are undistinguishable).
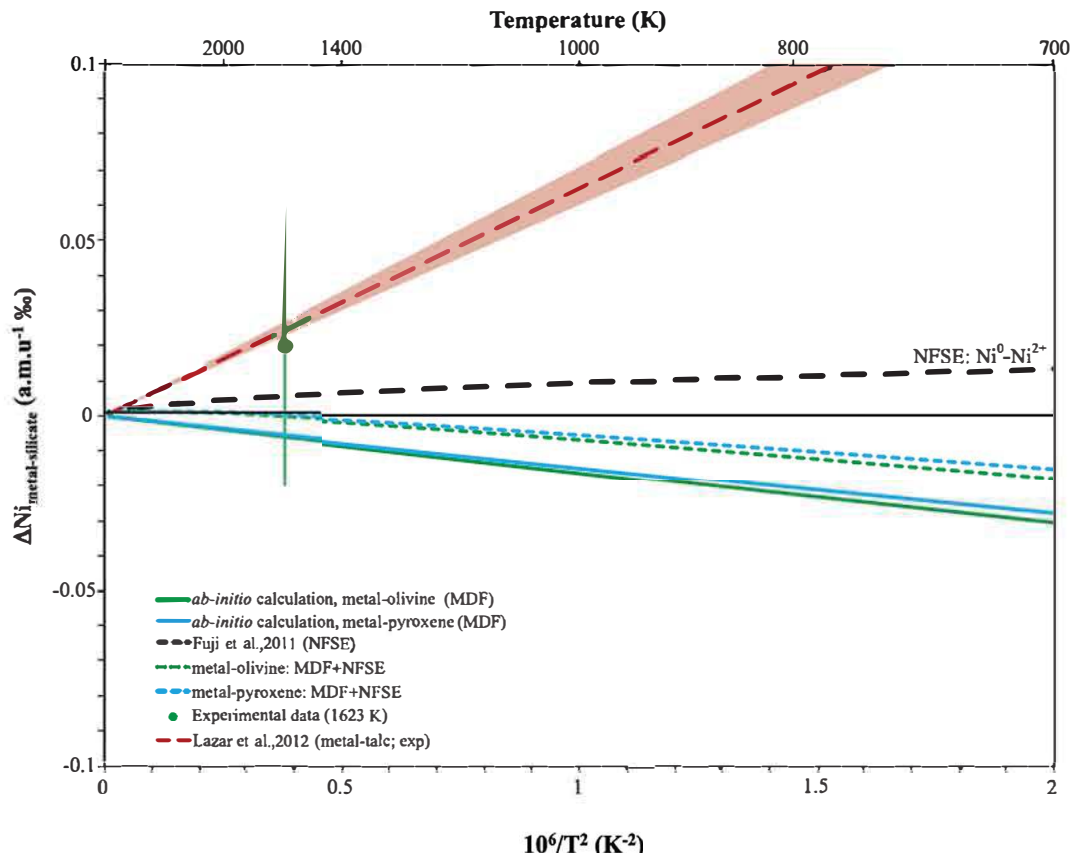
Fig. 5. Evolution of the metal silicate isotope fractionation factor at equilibrium (ΔNi in a.mu [1]) as a function of temperature. The metal olivine/pyroxene fractionation (Mass dependent fractionation, MDF) are found to be negative and extrapolation with temperature show a weak dependency. Experimental data on metal talc (Lazar et al., 2012) do not match our theoretical calculations. Conversely, our experimental data points on metal silicate melt at high temperature agrees with the calculations within error bars. Contribution of nuclear field shift effects (NFSE) has been calculated (Fuji et al., 2011) and is not significant relative to the total fractionation. Width of this curve shows the variability of this process for the different isotopes ratios.

temperatures from 1623 down to 1173 K (Lazar et al., 2012). Hence, at temperatures of metal silicate differentia tion, i.e. above the melting point of FeNi alloy relevant of planetesimals (1700 1800 K), no metal silicate fractiona tion of Ni isotopes would occur within attainable analytical precision. However, only talc has been investigated while this mineral is not representative of silicates found in mete orites. Conversely, the present study focuses on olivine and pyroxene, two of the major silicate phases of planetesimals.

At 1623 K, our experiments and calculations show respectively $\Delta Ni_{M-S} = 0.02 \pm 0.04\%.amu^{-1}$ and 0.006%. amu^{-1}, values that are in good agreement with those of Lazar ($\Delta Ni_{metal-talc} = 0.025 \pm 0.003\%o.amu^{-1}$) at the same temperature. Interestingly, metal talc nickel fractionation decreases with increasing temperature, while the metal olivine/pyroxene increases (Fig. 5). It is also more temper ature dependent in the case of the metal talc system (Fig. 5). This difference of behavior between olivine/pyrox ene and talc is not trivial to explain because Ni sites are sim ilar in these phases, the only difference being the presence of hydroxyl groups (OH) in talc. One explanation is that this is related to the inherent limits of the three isotopes method in the determination of equilibrium isotope fractionation for

metal oxide (or silicate) systems. As reviewed recently (Cao and Bao, 2017, Bourdon et al., 2018), this experimen tal approach may lead to incorrect equilibrium fractiona tion factors due to sufficiently accounted for kinetic effects in the three isotope diagram. Moreover, the use of a metallic capsule (gold in this case) directly in contact with a metallic sample introduces a third reservoir that may affect the isotope fractionation of interest. This finding was indeed a major result of the study of Lazar et al. (2012) that highlighted, for long run durations, kinetic effects caused by such interactions. Further experimental and theoretical investigations are required for nickel iso topes at low temperature (temperature range of 700 1300 K) to clarify the reasons for this discrepancy.

4.2. Kinetic isotope fractionation and diffusion processes

Mass dependent kinetic isotope fractionation in a metal silicate system can be due to different processes: (1) evapo ration; (2) chemical diffusion in a silicate melt; (3) grain boundary diffusion in solid silicates; (4) volume diffusion in metals; (5) thermal (Soret) diffusion in silicate melts. Noteworthy, thermal diffusion in melts is many orders of

magnitude faster than chemical diffusion (Richter et al., 2009). Whatever the process considered, light isotopes have a higher diffusion coefficient than heavier isotopes and migrate faster. Diffusion coefficients D_i and D_j of two isotopes i and j of a given element, respectively, can be related to the masses m_i and m_j of the isotopes as follows:

$$D_i/D_j = \left(m_i/m_j\right)^{\beta_{Diff}} \tag{8}$$

with β_{Diff} being the fractionation factor. The starting phase then becomes isotopically heavier, while the phase where Ni goes into is increasingly enriched in light isotopes. Diffusion processes explain for instance the Ni isotope signature of kamacite and taenite in iron meteorites (Quitté et al., 2006c; Dauphas et al., 2007): during cooling of the meteorite and exsolution of kamacite, Ni goes from the Ni poor kamacite into the Ni rich taenite, so that kamacite is isotopically heavier than taenite. Here, in our short duration experiments, a strong enrichment in light isotopes is observed in the silicate reservoir ($\delta Ni_S = 0.98 \pm 0.05‰$. amu^{-1} after 2 hours of heat treatment). This enrichment corresponds to a kinetic isotopic fractionation between metal and silicate ($\Delta Ni_{M-S} = 0.72 \pm 0.06‰.amu^{-1}$), that has a clear diffusive origin (Figs. 1 3 and Table 2).

The kinetic isotope fractionation of nickel (coupled with iron) has been studied during Fe Ni interdiffusion in the course of alloying these two metals at 1GPa and 1473 1673 K in a piston cylinder apparatus (Watson et al., 2016). *In situ* measurements performed by these authors show an even stronger enrichment in light isotopes near the interface between the two initial reservoirs ($\delta Ni = 12‰.amu^{-1}$), which is expected since local measurements unravel the spatial redistribution of isotopes along the diffusion profile. From these profiles, the magnitude of the kinetic effect can be modeled and parameterized (e.g., Oeser et al., 2015). Such modeling cannot be performed using our bulk measurements, however. In the present study, the interpretation of the data thus relies on the comparison of our nickel data with iron isotopes.

4.3. Comparison with results obtained on iron isotopes

Nickel and iron share similar chemical and crystal chemical properties. This assertion holds for metallic Ni and Fe as well as for their divalent cations. In this respect, we thus discuss our new results on Ni isotopes using insights from the larger body of literature available on iron isotopes.

Several experimental studies have been performed on metal silicate isotope fractionation of iron at equilibrium. In general, authors agree on the absence, within uncertainty, of iron fractionation between metal (solid or liquid) and silicate melt, at least at temperatures above 1523 1570 K, pressure from 1 bar to 7.7 GPa and oxygen fugacity from IW+3 to IW 2 (IW = Iron (Fe) Wüstite (FeO) buffer) (Roskosz et al., 2006; Poitrasson et al., 2009; Hin et al., 2012). This has also been shown at higher pressures using an alternative spectroscopic approach to determine fractionation factors (Liu et al., 2017). These experimental studies are in good agreement with meteorite investigations leading to the conclusion of the absence Fe isotope frac

tionation at equilibrium between metal and silicate under planetary core formation conditions (Poitrasson et al., 2005; Chernozhkin et al., 2016, 2017; Jordan et al., 2019). A recent study suggested, however, that the iron isotope fractionation factor becomes significant if a large amount of Ni is alloyed to iron (Elardo & Shahar, 2017). For low Ni contents of ca. 5%, compatible with planetary cores though, the metal silicate Fe isotope fractionation factor found in this study is not significantly different from 0‰. A more recent work from the same group investigated the effect of the abundance of the third potentially abundant element in planetary cores besides Fe and Ni, silicon, in the metal (Elardo et al., 2019). Here also, four out the five experiments produced did not generated notable Fe isotope fractionation between metal and silicate. The chemical composition dependence (e.g., the amount of Ti in the silicate) of iron isotopes fractionation is also in debate for olivine/silicate melt system in which no evidence of this dependence has been observed (Prissel et al., 2018).

In metal silicate systems with only iron as metal, the value of high temperature equilibrium fractionation (in amu^{-1}) between metal and silicate (ΔFe_{M-S}) is close to zero (i.e., $0.20 \pm 0.15‰$ in Roskosz et al., 2006; $0.016 \pm 0.021‰$ in Poitrasson et al., 2009, and $0.005 \pm 0.020‰$ in Hin et al., 2012). Our experimental data on nickel isotopes are similar to these Fe results, revealing no isotope fractionation at equilibrium at high temperature (typically $T > 1600$ K). Turning to the temperature dependence, experiments on Ni isotopes may also suggest a possible positive fractionation factor. Despite being too small to be confirmed experimentally, this issue may be discussed on the basis of our theoretical calculations. Reduced partition function ratios (β factors) of iron isotopes have already been determined (Fig. 4) for several minerals and amorphous silicates and also for metal (Alp et al., 2001; Tsunoda et al., 2002), olivine (Dauphas et al., 2012), pyroxene (Jackson et al., 2009), silicate glasses under reduced conditions (Dauphas et al., 2014) and spinel group minerals (Roskosz et al., 2015). The β factor of iron metal was always found to be lower than those of silicates, be they crystalline or amorphous, and even at high pressure (Liu et al., 2017). Moreover, the temperature dependence is more pronounced for iron than for nickel. It also appears that β factors of various silicates (olivine, pyroxene, basalt) are undistinguishable within uncertainty considering Fe or Ni isotopes (Fig. 4). This similarity is true only when iron exhibits a divalent state in silicates. This is another independent confirmation that Ni and Fe share common crystal chemical properties, including local vibrational properties controlling isotope fractionation. It allows also us to safely use our DFT calculation for Ni on crystalline olivine and pyroxene as reasonable proxies for the silicate melt of our experiments.

Regarding the isotope redistribution during diffusive processes involving metal and silicates, iron isotopes were first studied during diffusion between an iron doped silicate melt and a platinum metallic reservoir, using a similar experimental set up to that of the present study (Pt wire loop or Pt crucible), at 1500 °C, various fO_2 and from 30 minutes to 24 hours (Roskosz et al., 2006). In that case,

kinetic isotope fractionation was demonstrated to be driven by diffusion during the alloying of Fe (diffusing out of the silicate melt) with a platinum wire. A strong negative metal silicate kinetic fractionation was measured in that study ($\Delta Fe_{M\text{-}S} = 1.893 \pm 0.223‰.amu^{-1}$ after 30 minutes at 1500 °C and $fO_2 = 10^{-5}$ atm, *i.e.* around the Fe_3O_4 FeO buffer), a value nearly 3 times larger than in the present experiments on Ni (Table 2). In the former series of exper iments on Fe, kinetic fractionation depended on oxygen fugacity with a stronger fractionation at reducing condi tions, where the chemical disequilibrium between the metal and the silicate phase was the largest. Contrary to iron, fractionation of nickel isotopes appears to be insensitive to redox conditions (in the range studied here), as it remains only divalent in silicates. Roskosz et al. (2006) also per formed *in situ* measurements on these samples and showed that during diffusive processes from the silicate melt to the platinum reservoir, iron isotope fractionation between the core and the rim of the Pt wire can reach $14‰.amu^{-1}$. This magnitude is very similar to that recently reported for Fe Ni alloying (Watson et al., 2016), with a core rim iron iso tope fractionation in the nickel reservoir of $15‰.amu^{-1}$ under their experimental conditions (1GPa, 1473 1673 K, 24 240 h). Hence, diffusivity of iron isotopes into metals, i.e., diffusion driven fractionation, is similar in both sys tems (silicate melt and platinum in Roskosz et al., 2006, and iron metal and nickel metal in Watson et al., 2016). The exponent $\beta\delta_{iff}$ (Eq. (8)) linking isotope masses and dif fusivity are indeed similar in both studies, respectively 0.27 $\pm$ 0.04 and 0.32 $\pm$ 0.04, and are also similar in the case of nickel isotopes (0.30 ± 0.05 and 0.36 ± 0.05 at 1573 K and 1673 K, respectively, Watson et al., 2016). Again this comparison between results obtained for Ni and Fe indi cates very similar isotopic behavior of Ni and Fe when they are put under comparable conditions and supports the interpretation of Ni isotope data as reflecting kinetic pro cesses driven by diffusion processes.

Hence, our experiments and theoretical calculations shows that under conditions where Fe and Ni are both metallic or divalent, these two elements share isotope equi librium fractionation factors and diffusional processes per atomic mass unit.

4.4. Application to natural samples

Experimental work allows determining whether equilib rium has been reached in the samples or not. This is of major importance, as isotopic signatures can be used as geothermometers in cases where systems equilibrated, hav ing thus the potential to shed thus light on the thermal his tory of the meteorite parent body. Furthermore, diffusion profiles provide constraints on the cooling rate history in cases where full equilibrium has not been achieved.

In natural samples, nickel stable isotopes were first mea sured in the metallic fraction of chondrites and in iron meteorites (Cook et al., 2007; Moynier et al., 2007). Note that the standard used by Moynier et al. (2007) is undistin guishable from SRM 986 and therefore their results are comparable to others. In chondrites, metal fraction and bulk samples show δNi values in the same range, from

0.080 to $0.440‰.amu^{-1}$ (Moynier et al., 2007; Cameron et al., 2009; Steele et al., 2011; Gueguen et al., 2013; Chernonozhkin et al., 2016; Gall et al., 2017; see Fig. 6). This is completely expected as the Ni budget is at 99% in the metal. Moreover, chondrites are known to have experi enced moderate heating through thermal metamorphism from 800 to 1300 K, i.e. without any melting. At these con ditions of temperature, our DFT calculations predict barely measurable metal silicate fractionation of Ni isotopes between 0.022 and $0.009‰.amu^{-1}$ (Fig. 5). Measurements on the silicate part of chondrites would thus be of major importance to determine if these samples formed in equilib rium or not.

Similarly, iron meteorites display Ni isotope composi tion of $\delta^{60}Ni = 0.050$ to $0.323‰.amu^{-1}$ (Chernonozhkin et al., 2015, Gall et al., 2017). Chondrites and iron meteorites have therefore an equivalent range of Ni isotopic compositions indicating that core formation processes are not accompanied by Ni isotope fractionation. This conclusion is perfectly in line with the interpretation of Gall et al. (2017) and is also supported by our experimental and theoretical results.

Cook et al. (2007) were the first ones to measure Ni iso topes in the metal phase of a few pallasites; they observed a variability between 0.10 and $0.10‰.amu^{-1}$ (Fig. 6). This variability was confirmed and enhanced by complementary measurements by Chernonozhkin et al. (2016, 2017), who analyzed Fe and Ni stable isotopes in pallasites and meso siderites, two types of differentiated meteorites made of both metal and silicates. In pallasites, Ni and Fe isotope fractionation are similar in magnitude and opposite in sign. Different formation scenarios are invoked for pallasites: these meteorites either sample the mantle core boundary of a differentiated body and result from magmatic processes (e.g. Wasson and Choi, 2003; McKibbin et al., 2016 and references therein), or they formed by impacts between already differentiated planetesimals (Scott, 2007; Solferino et al., 2015; Solferino and Golabek, 2018). Nickel and Fe isotopes data can be discussed relative to these different processes. Both elements have similar condensation temper atures; impact induced evaporation processes should then affect both of them in the same way. Besides, our experi ments suggest that evaporation processes induce no Ni iso topes fractionation between metal and silicate (Fig. 3a). Evaporation / recondensation is therefore not the dominant process responsible for the observed isotope signatures of metal and silicate in pallasites.

According to Chernonozhkin et al. (2016), the Fe iso tope signature is due to a later stage Fe isotopic re equilibration between metal and silicate, rather than a pris tine record of mantle core differentiation. Iron isotope frac tionation measured between metal and olivine possibly reflected a final equilibration at 1273 K for some pallasites, whereas others were clearly out of isotopic equilibrium (Poitrasson et al., 2005). For Ni, the metal is systematically isotopically lighter than olivine (Fig. 6). The negative metal silicate fractionation, ranging from $1.02 \pm 0.08‰.amu^{-1}$ to $0.10 \pm 0.04‰.amu^{-1}$, cannot be explained by our experimental results on equilibrated samples at high tem perature. For temperatures higher than 700 K, our DFT
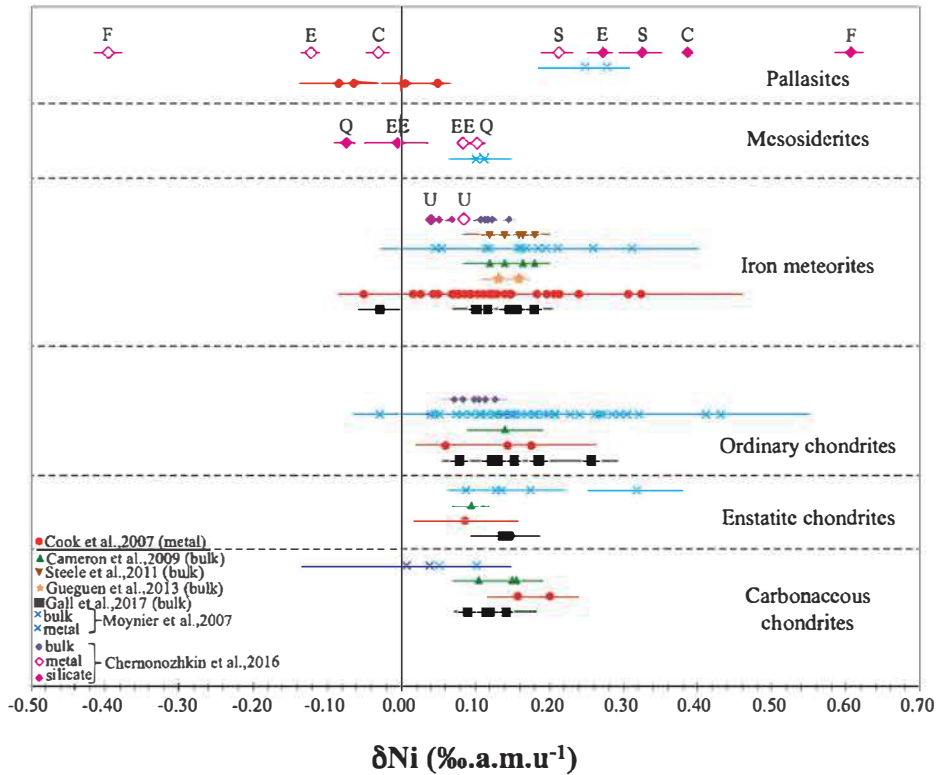
Fig. 6. Compilation of nickel isotopes composition in different types of meteorites. Measurements were made on either bulk samples, on the metallic phase or on separate silicate minerals (see inset for references). All measurements are relative to NIST SRM 986 except in Moynier et al. (2007), where δNi values are calculated relative to Aesar ICP MS standard (Batch No 066110910). Noteworthy, the isotope composition of both standards is the same within uncertainty. Letters above points represent meteorites in which both metal and silicate have been measured. F: Fukang; E: Esquel; C: CMS 04071; S: Seymchan; EE: EET 8750,51; Q: QUE 93001,23; U: Udei Station.

calculations suggest an evolution of equilibrium fractiona tion from 0.03‰.amu⁻¹ to values very close to zero (Fig. 5), a range that is far from the very negative fraction ation measured in pallasites. It thus appears that the Ni iso tope signatures between metal and silicate do not represent a high temperature isotopic equilibrium in pallasites. Other features support this conclusion of disequilibrium in palla sites. First, textures of olivines (angular vs. rounded) have been studied to estimate the degree of equilibrium of palla sites (Ohtani, 1983). It has been experimentally shown that it could take between 50 to 2000 years to round an olivine with a radius of 100 μm in a FeNi matrix at temperatures between 1473 and 1673 K whereas 7 200 Ma are required for 5 mm grains as typically observed in pallasites (Sakai et al., 2003). Finally, the occurrence of diffusion profiles from core to rim in olivine grains for several minor elements including Ni (as well as Ca, Cr, Ti, V, W) in different pall asites suggests cooling rates from high temperatures of sev eral hundred degrees per million years (Miyamoto, 1997; Hsu, 2003; Quitté et al., 2005), preventing these rocks from being texturally, isotopically and compositionally equili brated. If pallasites did not reach equilibrium or are not at equilibrium anymore, Ni isotope fractionation in these meteorites cannot be used as a geothermometer. The Ni iso tope fractionation observed in pallasites is most likely explained by sub solidus solid state diffusion of Ni from oli vine into metal during cooling. The absolute value of ΔNi_{M-}

$_S$ (0.105 0.417‰.amu⁻¹, Chernonozhkin et al., 2016) is indeed compatible with the kinetic isotope fractionation determined in the present study, except for the Fukang pal lasite that displays an extreme absolute value of 1.016‰. amu⁻¹. Note that the wide range of ΔNi_{M-S} observed between pallasite samples is most likely related to the kamacite/taenite ratio in the samples considered as "bulk metal". Indeed, using in situ LA MC ICP MS measure ments, Chernonozhkin et al. (2017) determined isotope ratio profiles across kamacite taenite interfaces with a $\Delta Ni_{kam-tae} = +1.59$ to $+2.50$‰. They also pointed out a vari ability of ca. 0.7‰ between the different data points of kamacite in Esquel pallasite, and ca. 1.0‰ for taenite in the same meteorite. The direction of Ni metal silicate iso topic fractionation in pallasites is however opposite of what was found in our experiments (Fig. 3). It is generally expected that diffusion operates because of a difference of concentration in the element of interest, with diffusion from the more concentrated phase to the least concentrated (e.g. Richter et al., 2009). Hence Ni diffusion is expected from the metal into olivine. Nevertheless, the measured ΔNi_{M-S} values rather suggest that in the case of pallasites, Ni diffu sion occurred from silicates into metal alloy leading to an enrichment of the metal phase in light isotopes and result ing in a silicate isotopically heavier. This is likely due to the increase of the metal silicate partition coefficient of Ni ($D_{met/sil}$) with decreasing temperature along the IW buffer

(Capobianco and Amelin, 1994). In other words, Ni becomes more siderophile and therefore, Ni naturally diffuses from silicates to the metal alloy upon cooling, thereby explaining the isotopic observations. The large isotope fractionation of Ni between both phases also indicates that the cooling rate of pallasites was relatively low to ensure enough time for sub solidus to take place. Modeling such diffusion would help to provide quantitative discussion on thermal history and in particularly on cooling rate of pallasites parent body but a detailed modeling is out of the scope of the present manuscript. It is however possible to conclude that pallasites have a core mantle boundary origin followed by slow cooling rates rather than higher ones as expected in impact induced processes.

In mesosiderites, metal and silicates display a much more limited isotope fractionation of nickel isotopes with $\Delta Ni_{M-S} = 0.073 \ 0.170‰.amu^{-1}$ (Chernonozhkin et al., 2016) whereas our experimental and calculated fractionation at equilibrium is $0.02 \pm 0.04‰.amu^{-1}$ and $0.005‰.amu^{-1}$ respectively (Fig. 5). Contrary to pallasites, metal is isotopically slightly heavier than silicate and mesosiderites are characterized by an apparent positive metal silicate fractionation of nickel isotopes (Fig. 6). Besides, mesosiderites silicates are also slightly enriched in light iron isotopes relative to the metal phase. The similar behavior of Fe and Ni has been interpreted as resulting from a limited diffusion of Fe and Ni from metal into silicates (Chernonozhkin et al., 2016), due to an evolution of oxygen fugacity conditions in the parent body, in particularly towards more oxidizing conditions. Mesosiderites have had a complex multi stage history including disruption of the parent body and re accretion. A rapid cooling rate at high temperature prevents diffusion processes to be as efficient as in pallasites that experienced slower cooling rates. Hence, despite their complex history, mesosiderites are apparently closer to equilibrium than pallasites in terms of Fe and Ni isotope compositions.

5. CONCLUSION

Kinetic and equilibrium nickel isotope fractionations between metal and silicate have been investigated experimentally and by DFT calculations. Experimental data show that chemical equilibrium is a function of oxygen fugacity, and is reached after 1 and 17 hours of annealing, for experiments at a fO_2 $10^{-8.2}$ and $10^{-9.9}$ atm. respectively. The diffusion process generates a strong isotope fractionation with a transient enrichment of light isotopes in the silicate melt at the beginning of the experiments. After 24 hours of heat treatment, isotopic equilibrium is reached and no metal silicate fractionation is observed within uncertainties at temperatures relevant to metal silicate differentiation. This result is also supported by DFT calculations on metal olivine and metal pyroxene that additionally show a weak temperature dependence of this fractionation. At equilibrium, comparison of these data and those obtained for iron under similar conditions are very similar suggesting a comparable isotopic behavior for both Ni and Fe during igneous processes. Finally, comparison with natural samples shows that metal silicate fractionation in mesosiderites

and pallasites is most likely the result of diffusion driven processes instead of reflecting equilibrium isotopic fractionations. This would result in an undisturbed thermal history of these bodies, at least down to temperatures were diffusion is no more efficient, creating the observed diffusion profiles. In pallasites, the reverse isotope fractionation between silicates and metal (relative to the experimental work) is associated with diffusion of Ni from silicates into metal during cooling, when Ni becomes more siderophile.

The same approach applied to partially differentiated primitive achondrites such as acapulcoites and lodranites, i.e., the comparison between experimental results and measured isotope fractionation between metal and silicate of natural samples, will therefore help us to elucidate the thermal history of their parent body and the processes (equilibrium vs. diffusion driven) involved in their metal silicate differentiation.

Declaration of Competing Interest

The authors declare that they have no known competing financial interests or personal relationships that could have appeared to influence the work reported in this paper.

APPENDIX. COMPARISON OF CALCULATED STRUCTURAL AND VIBRATIONAL PROPERTIES WITH EXPERIMENT, AND DISCUSSSION OF THE NUMERICAL ERRORS

The structural, vibrational and fractionation properties of Ni metal, Ni olivine (Liebenbergite Ni_2SiO_4), and Ni diopside have been computed by ab initio calculations. In the case of Liebenbergite, we tested the effect of various numerical parameters and physical frameworks. More precisely, we tested the effect of the magnetic structure, and the importance of taking into account the phonon dispersion. Due to limitations of our numerical framework, we were not able to assess dielectric and Born effective charges in the present work. Indeed, in the current implementation of the PWSCF code and for spin polarized systems (i.e. all of our systems), these dielectric quantities cannot be directly computed by linear response. This, together with the incompleteness of experimental frequencies, has limited us in the precise comparison of our calculated frequencies

Table A1

Lattice parameters and selected structural parameters of Ni metal, Liebenbergite and Ni diopside, compared with experiment (Exp) and previous calculations (PBE). The numbers in parenthesis refer to uncertainties on the last significant digit.

Ni metal	This work	Δ th/exp	PBE ([b])				Exp([a])
a (Å)	3.518	+0.1%	3.514				3.513[5]

Liebenbergite	This work calc.([d])	Δ th/exp	calc.([e])	Δ th/exp	calc.([f])	Δ th/exp	Exp([c])
a (Å)	4.7614	+0.7%	4.7679	+0.8%	4.7587	+0.6%	4.7296[3]
b (Å)	10.2875	+1.6%	10.2427	+1.2%	10.2769	+1.5%	10.1209[6]
c (Å)	5.9533	+0.6%	5.9594	+0.8%	5.9546	+0.7%	5.9150[4]
γ (°)	90		90.00001		90.00006		90

Ni diopside	This work([g])	Δ th/exp	Exp([h]):
a (Å)	9.9015	+1.7%	9.7359[4]
b (Å)	9.0161	+1.4%	8.8932[4]
c (Å)	5.3027	+1.4%	5.2284[3]
β (°)	106.320		105.830[3]

[a] Kresch et al. (2007) neutron diffraction at 10 K.
[b] Lee et al. (2006).
[c] Bostrom (1987), X ray diffraction at ambient temperature.
[d] Simple antiferromagnetic state with antiparallel M1 and M2 spins.
[e] Antiferromagnetic state c1 following Cococcioni et al. (2003).
[f] Antiferromagnetic state c2 following Cococcioni et al. (2003).
[g] Ferromagnetic state.
[h] Raudsepp et al. (1990), X ray diffraction at ambient temperature.

with experimental data, therefore in the assessment of the quality of our calculations. The potential effect of dielectric tensor and effective charges on fractionation properties was assessed on the Mg β factor of forsterite Mg_2SiO_4 (calculation of Méheut et al. (2009)), and was found to be negligible (0.3% of its $\ln\beta$ value in‰, essentially undistinguishable from expected numerical uncertainty). Further, the assessment of these quantities is the subject of a work in preparation, aiming at completing the present theoretical work.

A.1. Structural properties

The relaxed structures of the materials studied in this work are presented in Table A1 and A2. For Ni metal, the calculated cell parameter is in excellent agreement with the experimental value (Kresch et al., 2007), and with previous theoretical studies (Lee et al., 2006). This behavior seems relatively common for gradient corrected calculations of pure metals (Al: Dal Corso et al., 1996; Fe: Dal Corso and de Gironcoli, 2000; Au: Dal Corso et al., 1997). This contrasts with previous similar calculations on silicates, and on ionic insulators in general, which show 1 2% overestimate of cell parameters (see e.g. Méheut et al., 2007, 2009; Méheut and Schauble, 2014). For Liebenbergite or Ni diopside, the calculation is showing good agreement with this 1 2% overestimate. In particular, the different magnetic structures tested result in virtually identical structures.

A.2. Fractionation properties: metal and Ni-olivine

Computed β factors for metal and Ni olivine are shown on Fig. A1b. For Ni olivine, consistently with structural parameters (see above), the different magnetic structures

Table A2

Liebenbergite, Ni diopside: computed relaxed structure in reduced coordinates.

x/a		y/b	z/c
Liebenbergite[a]			
Ni(1)	0.00000	0.00000	0.00000
Ni(2)	0.99200	0.27374	0.25000
Si	0.42570	0.09408	0.25000
O(1)	0.76932	0.09490	0.25000
O(2)	0.28290	0.94456	0.25000
O(3)	0.27235	0.16224	0.02816
Ni diopside[b]			
M(1)	0.00000	0.90822	0.25000
M(2)	0.00000	0.29437	0.25000
T	0.28713	0.09266	0.22741
O(1)	0.11591	0.08700	0.14235
O(2)	0.36083	0.24990	0.31997
O(3)	0.35075	0.01773	0.99442

[a] Simple antiferromagnetic state with antiparallel M1 and M2 spins.
[b] Ferromagnetic state.

show very small difference in their β factors (corresponding to 0.9% of their $\ln\beta$ value in‰). In fact, these very small differences cannot reasonably be distinguished from expected numerical uncertainty. Interestingly, the β factor of the metallic phase shows very close to Ni olivine. This is quite surprising given the difference in the redox state, and more generally the difference between the bonds present in these two materials. In terms of metal silicate fractionation (Fig. A1a), because the β factors of metal and olivine are so close, the contrast between the different magnetic structures of olivine is subsequently amplified. We considered
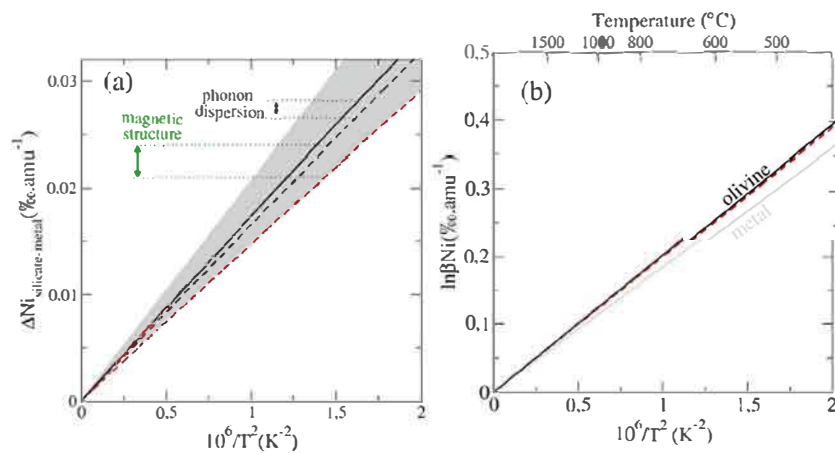
Fig. A1. Left: Ni olivine metal fractionation of Ni isotopes. Right: Ni isotopes β factors of Ni olivine and metal. Plain curves: calculations with phonon dispersion effects (Eqs. (8) and (16) of M'eheut et al. (2007)). Dashed lines: calculations for which the silicate β factor was computed with Γ point only phonon frequencies (Eq. (5) of Dupuis et al. (2015)). Black lines: cl antiferromagnetic structure. Red lines: simple antiferromagnetic structure. The c2 antiferromagnetic structure calculation is indistinguishable from the simple antiferromagnetic structure, and was not represented here. Grayed area: estimated numerical error, given by the difference between the reference curve (black plain line) and the more offset one (red dashed curve). Fitted to $\pm 0.0025 \frac{10^6}{T^2}$ (in‰.amu^{-1}).

these variations as an indication of the numerical uncer tainty of our calculated metal Ni olivine fractionation, rep resented by the grayed area on Fig. A1a. To assess the effect of phonon dispersion, we compared a calculation based on Γ point frequencies (dashed black curve on Fig. A1a) with a calculation based on a 2 × 2 × 2 phonon grid (plain black curve on Fig. A1a). Here also, the effect is within numerical uncertainty (0.4% of lnβ value in‰). In the following, the calculation with magnetic structure cl and dispersion effects (plain black line in Fig. A1) was considered as reference, for its slightly better agreement with experimental structural parameters, in particular for the angle β (see Table A1).

REFERENCES

Alp E. E. et al. (2001) Lattice dynamics and inelastic nuclear resonant X ray scattering. *J. Phys.: Condens. Matter* 13, 7645 7658.

Baronas J. J., Torres M. A., West A. J., Rouxel O., Georg B., Bouchez J., Gaillardet J. and Hammond D. E. (2018) Ge and Si isotope signatures in rivers: A quantitative multi proxy approach. *Earth Planet. Sci. Lett.* 503, 194 215.

Baroni S., de Gironcoli S. and Dal Corso A. (2001) Phonons and related crystal properties from density functional theory. *Rev. Mod. Phys.* 73, 515 562.

Bonnand P., Williams H. M., Parkinson I. J., Wood B. J. and Halliday A. N. (2016) Stable chromium isotopic composition of meteorites and metal silicate experiments: Implications for fractionation during core formation. *Earth Planet. Sci. Lett.* 435, 14 21.

Bostrom D. (1987). Single crystal X ray diffraction studies of synthetic Ni Mg olivine solid solutions 72, 965.

Bourdon B., Roskosz M. and Hin R. C. (2018) Isotope tracers of core formation. *Earth Sci. Rev.* 181, 61 81.

Cameron V., Vance D., Archer C. and House C. H. (2009) A biomarker based on the stable isotopes of nickel. *PNAS* 106, 10944 10948.

Cao X. and Bao H. (2017) Redefining the utility of the three isotopes method. *Geochim. Cosmochim. Acta.* https://doi.org/10.1016/j.gca.2017.05.028.

Capobianco C. J. and Amelin A. A. (1994) Metal silicate partitioning of nickel and cobalt: The influence of temperature and oxygen fugacity. *Geochim. Cosmochim. Acta* 58, 125 140.

Chernonozhkin S. M., Goderis S., Lobo L., Claeys P. and Vanhaecke F. (2015) Development of an isolation procedure and MC ICP MS measurement protocol for the study of stable isotope ratio variations of nickel. *J. Anal. At. Spectrom.* 30, 1518 1530.

Chernonozhkin S. M., Goderis S., Costas Rodriguez M., Claeys P. and Vanhaecke F. (2016) Effect of parent body evolution on equilibrium and kinetic isotope fractionation: a combined Ni and Fe isotope study of iron and stony iron meteorites. *Geochim. Cosmochim. Acta.* https://doi.org/10.1016/j.gca.2016.04.050.

Chernonozhkin S. M., Weyrauch M., Goderis S., Oeser M., McKibbin S. J., Horn I., Hecht L., Weyer S., Claeys P. and Vanhaecke F. (2017) Thermal equilibration of iron meteorite and pallasites parent bodies recorded at the mineral scale by Fe and Ni isotope systematics. *Geochim. Cosmochim. Acta* 217, 95 111.

Cococcioni M. and de Gironcoli S. (2005) Linear response approach to the calculation of the effective interaction param eters in the LDA+ U method. *Phys. Rev. B* 71, 035105.

Cococcioni M., Dal Corso A. and de Gironcoli S. (2003) Structural, electronic, and magnetic properties of Fe2SiO4 fayalite: Comparison of LDA and GGA results. *Phys. Rev. B* 67, 094106.

Cook D. L., Wadhwa M., Clayton R. N., Dauphas N., Janney P. E. and Davis A. M. (2007) Mass dependent fractionation of nickel isotopes in meteoritic metal. *Meteorit. Planet. Sci.* 42, 2067 2077.

Dal Corso A. and de Gironcoli S. (2000) Ab initio phonon dispersions of Fe and Ni 62, 273 277.

Dal Corso A., Pasquarello A. and Baldereschi A. (1996). Gener alized gradient approximation to density functional theory: a comparative study for atoms and solids 53, 1180.

Dal Corso A., Pasquarello A. and Baldereschi A. (1997) Density functional perturbation theory for lattice dynamics with ultra soft pseudopotentials. *Phys. Rev. B* 56, R11369 R11372.

Dauphas N. (2007) Diffusion driven kinetic isotope effect of Fe and Ni during formation of the Widmanstatten pattern. *Meteorit. Planet. Sci.* 42, 1597 1614.

Dauphas N., Roskosz M., Alp E. E., Golden D. C., Sio C. K., Tissot F. L. H., Hu M. Y., Zhao J., Gao L. and Morris R. V. (2012) A *general moment* NRIXS approach to the determina tion of equilibrium Fe isotopic fractionation factors: Applica tion to goethite and jarosite. *Geochim. Cosmochim. Acta* **94**, 254 275.

Dauphas N., Roskosz M., Alp E. E., Neuville D. R., Hu D. R., Sio C. K., Tissot F. L. H., Zhao J., Tissandier L., Medard E. and Cordier C. (2014) Magma redox and structural controls on iron isotope variations in Earth's mantle and crust. *Earth Planet. Sci. Lett.* **398**, 127 140.

Dingwell D. B., O'Neill H. S. T. C., Ertel W. and Spettel B. (1994) The solubility and oxidation state of nickel in silicate melt at low oxygen fugacity: Results using mechanically assisted equilibrium technique. *Geochicm. Cosmochim. Acta* **58**, 1967 1974.

Dupuis R., Benoit M., Nardin E. and Mheut M. (2015) Fraction ation of silicon isotopes in liquids: The importance of config urational disorder. *Chem. Geol.* **396**, 239 254.

Durand G., Vilminot S., Rabu P., Derory A., Lambour J. P. and Ressouche E. (1996) Synthesis, structure, and magnetic prop erties of CaMSi$_2$O$_6$(M=Co, Ni) compounds and their solid solutions. *J. Solid State Chem.* **124**, 374 380.

Elardo S. M. and Shahar A. (2017) Non chondritic iron isotope ratios in planetary mantles as a result of core formation. *Nat. Geosci.* **10**, 317 321.

Elardo S. M., Shahar A., Mock T. D. and Sio C. K. (2019) The effect of core composition on iron isotope fractionation between planetary cores and mantles. *Earth Planet. Sci. Lett.* **513**, 124 134.

Fuji T., Moynier F., Dauphas N. and Abe M. (2011) Theoretical and experimental investigation of nickel isotopic fractionation in species relevant to modern and ancient oceans. *Geochim. Cosmochim. Acta* **75**, 469 482.

Gall L., Williams H. M., Halliday A. N. and Kerr A. C. (2017) Nickel isotopic composition of the mantle. *Geochim. Cos mochica Acta* **199**, 196 209.

Garrity K. F., Bennett J. W., Rabe K. M. and Vanderbilt D. (2014) Pseudopotentials for high throughput DFT calculations. *Com put. Mater. Sci.* **81**, 446 452.

Georg R. B., Halliday A. N., Schauble E. A. and Reynolds B. C. (2007) Silicon in the Earth's core. *Nature* **447**, 1102 1106.

Giannozzi P., Baroni S., Bonini N., Calandra M., Car R., Cavazzoni C., Ceresoli D., Chiarotti G. L., Cococcioni M., Dabo I., Corso A. D., de Gironcoli S., Fabris S., Fratesi G., Gebauer R., Gerstmann U., Gougoussis C., Kokalj A., Lazzeri M., Martin Samos L., Marzari N., Mauri F., Mazzarello R., Paolini S., Pasquarello A., Paulatto L., Sbraccia C., Scandolo S., Sclauzero G., Seitsonen A. P., Smogunov A., Umari P. and Wentzcovitch R. M. (2009) QUANTUM ESPRESSO: a modular and open source software project for quantum simu lations of materials. *J. Phys.: Condens. Matter* **21**, 395502.

Gueguen B., Rouxel O., Ponzera E., Bekker A. and Fouquet Y. (2013) Nickel stable isotope variations in terrestrial silicate rocks and geological reference materials measured by MC ICP MS. *Geostand. Geoanal. Res.* **37**, 297 317.

Gueguen B., Rouxel O., Rouget M. L., Bollinger C., Ponzera E., Germain Y. and Fouquet Y. (2016) Comparative geochemistry of four ferromanganese crusts from Pacific ocean and signifi cance for the use of Ni isotopes as paleoceanograhic tracers. *Geochim. Cosmochim. Acta* **189**, 214 235.

Hagemann I. S., Khalifah P. G., Ramirez A. P. and Cava R. J. (2000) Geometric magnetic frustration in olivines. *Phys. Rev. B* **62**, R771 R774.

Hin R. C., Schmidt M. W. and Bourdon B. (2012) Experimental evidence for the absence of iron isotope fractionation between metal and silicate liquids at 1 GPa and 1250 1300°C and its cosmochemical consequences. *Geochim. Cosmochim. Acta* **93**, 164 181.

Hin R. C., Burkhardt C., Schmidt M. W., Bourdon B. and Kleine T. (2013) Experimental evidence for Mo isotope fractionation between metal and silicate liquids. *Earth Planet. Sci. Lett.* **379**, 38 48.

Hohenberg P. and Kohn W. (1964) Inhomogeneous electron gas. *Phys. Rev.* **136**, 864 871.

Hohl S. V., Galer S. J. G., Camper A. and Becker H. (2015) Cadmium isotope variations in Neoproterozoic carbonates A tracer of biologic production ? *Geochem. Perspect. Lett.* **3**, 32 44.

Hsu W. (2003) Minor element zoning and trace element geochem istry of pallasites. *Meteorit. Planet. Sci.* **38**, 1217 1241.

Jackson J. M., Hamecher E. A. and Sturhahn W. (2009) Nuclear resonant X ray spectroscopy of (Mg, Fe)Si$_O$3 orthoenstatites. *Eur. J. Mineralalogy* **21**, 551 560.

Jordan M. K., Tang H. L., Kohl I. E. and Young E. D. (2019) Iron isotope constraints on planetesimal core formation in the early solar system. *Geochim. Cosmochim. Acta* **246**, 461 477.

Kempl J., Vroon P. Z., van der Wagt B., Zinngrebe E., Frost D. J. and van Westrenen W. (2016) Silicon stable isotope fraction ation between metal and silicate at high pressure, high temper ature conditions as a tracer of planetary core formation. *Neth. J. Geosci.* **95**, 113 129.

Klayer M. and Elliott T. (2018) Non chondritic Ni isotope composition of the bulk silicate earth. *Lunar and Planetary Science Conference, Abstract #4035*.

Kohn W. and Sham L. (1965) Self consistent equations including exchange and correlation effects. *Phys. Rev.* **140**, A1133 A1138.

Kresch M., Delaire O., Stevens R., Lin J. Y. Y. and Fultz B. (2007) Neutron scattering measurements of phonons in nickel at elevated temperatures. *Phys. Rev. B* **75**, 104301.

Lazar C., Young E. D. and Manning C. E. (2012) Experimental determination of equilibrium nickel isotope fractionation between metal and silicate from 500 °C to 950 °C. *Geochim. Cosmochim. Acta* **86**, 276 295.

Lee J. H., Hsue Y. C. and Freeman A. J. (2006) Magnetically induced variations in phonon frequencies. *Phys. Rev. B* **73**, 172405.

Lejaeghere K. et al. (2016) Reproducibility in density functional theory calculations of solids. *Science* **351**, 6280.

Liu J., Dauphas N., Roskosz M., Hu M. Y., Yang H., Bi W., Zhao J., Alp E. E., Hu J. Y. and Lin J. F. (2017) Iron isotopic fractionation between silicate mantle and metallic core at high pressure. *Nat. Commun.* **8**, article 14377.

Luais B. (2007) Isotopic fractionation of germanium in iron meteorites: Significance for nebular condensation, core forma tion and impact processes. *Earth Planet. Sci. Lett.* **262**, 21 36.

Mahan B., Siebert J., Pringle E. A. and Moynier F. (2017) Elemental partitioning and isotopic fractionation of Zn between metal and silicate and geochemical estimation of the S content of the Earth's core. *Geochim. Cosmochim. Acta* **196**, 252 270.

McKibbin, S., Ireland, T., O'Neill, H., Holden, P., Mallmann, G., and Claeys, P. (2016). Rapid Planetesimal cooling after core formation: Pallasite meteorites. EGUGA1815284M.

McManus J., Nagler T. F., Siebert C., Wheat C. G. and Hammond D. E. (2002) Oceanic molybdenum isotope fractionation: Diagenesis and hydrothermal ridge flank alteration. *Geochem., Geophys., Geosyst.* **3**, 1078.

Méheut M., Lazzeri M., Balan E. and Mauri F. (2007). Equilib rium isotopic fractionation in the kaolinite, quartz, water system: predictions from first principles density functional the ory 71, pp. 3170 3181.

Méheut M., Lazzeri M., Balan E. and Mauri F. (2009). Structural control over equilibrium silicon and oxygen isotopic fraction ation: A first principles density functional theory study 258, 28 37. Applications of non traditional stable isotopes in high temperature geochemistry.

Méheut M., Lazzeri M., Balan E. and Mauri F. (2007) Equilibrium isotopic fractionation in the kaolinite, quartz, water system: predictions from first principles density functional theory. *Geochim. Cosmochim. Acta* **71**, 3170 3181.

Méheut M. and Schauble E. A. (2014) Silicon isotope fractionation in silicate minerals: Insights from first principles models of phyllosilicates, albite and pyrope. *Geochim. Cosmochim. Acta* **134**, 137 154.

Miyamoto M. (1997) Chemical zoning in several pallasites. *J. Geophys. Res.* **102**, 21613 21618.

Moynier F., Blichert Toft J., Telouk F., Luck J. M. and Albarede F. (2007) Comparative stable isotope of N, Cu, Zn and Fe in Chondrites and iron meteorites. *Geochim. Cosmochim. Acta* **71**, 4365 4379.

Noordmann J., Weyer S., Georg B. R., Jons S. and Sharma M. (2015) $^{238}U/^{235}U$ isotope ratios of crustal material, rivers and products of hydrothermal alteration: new insights on the oceanic U isotope mass balance. *Isot. Environ. Health Stud.* **52**, 141 163.

Oeser M., Dohmen R., Horn I., Schuth S. and Weyer S. (2015) Processes and time scales of magmatic evolution as revealed by Fe Mg chemical and isotopic zoning in natural olivines. *Geochim. Cosmochim. Acta* **154**, 130 150.

Ohtani E. (1983) Formation of olivine textures in pallasites and thermal history of pallasites in their parent body. *Phys. Earth Planet. Inter.* **32**, 182 192.

Perdew J. P., Burke K. and Ernzerhof M. (1996) Generalized gradient approximation made simple. *Phys. Rev. Lett.* **77**, 3865 3868.

Petry C., Palme H. and Chakraborty S. (1996) Nickel content in oxidized meteorites as an indicator of thermal history A preliminary report. *Meteorit. Planet. Sci.* **31**, A107.

Poitrasson F., Levasseur S. and Teutsch N. (2005) Significance of iron isotope mineral fractionation in pallasites and iron meteorites for the core mantle differentiation of terrestrial planets. *Earth Planet. Sci. Lett.* **234**, 151 164.

Poitrasson F., Roskosz M. and Corgne A. (2009) No iron isotope fractionation between molten alloys and silicate to 2000 °C and 7.7 GPa: Experimental evidence and implicationsfor planetary differentiation and accretion. *Earth Planet. Sci. Lett.* **278**, 376 385.

Prissel K. B., Krawczynski M. J., Nie N. X., Dauphas N., Couvy H., Hu M. Y., Alp E. E. and Roskosz M. (2018) Experimentally determined effects of olivine crystallization and melt titanium content on iron isotopic fractionation in planetary basalts. *Geochim. Cosmochim. Acta* **238**, 580 598.

Quitté G., Birck J. L. and Allègre C. J. (2005) Stony iron meteorites: History of the metal phase according to tungsten isotopes. *Geochim. Cosmochim. Acta* **69**, 1321 1332.

Quitté G., Meyer M., Latkoczy C., Halliday A. N. and Gunther D. (2006b) Nickel isotopes in iron meteorites nucelosynthetic anomalies in sulphides with no effects in metals and no trace of 60Fe. *Earth Planet. Sci. Lett.* **242**, 16 25.

Quitté G. and Oberli F. (2006) Quantitative extraction and high precision isotope measurements of nickel by MC ICPS. *J. Anal. At. Spectrom.* **21**, 1249 1255.

Quitté G., Halliday A. N., MArkowski A., Bourdon B., Meyer B., Zanda B., Latkoczy C. and Guenther D. (2006a) Ni isotopes in the early solar system: an overview. *American Geophysical Union, Fall Meeting, abstract*, V12A 0548.

Quitté G., Latkoczy C., Schonbachler M., Halliday A. N. and Gunther D. (2011) 60Fe 60Ni systematics in the eucrites parent body: A case study of Bouvante and Juvinas. *Geochim. Cosmochica Acta* **75**, 7698 7706.

Quitté G., Poitrasson F. and Guignard J. (2017) Nickel isotopes as a tracer of planetary differenciation processes? *Goldschmidt Conference, Abstract*, #3254.

Ratié G., Jouvin D., Garnier J., Rouxel O., Miska S., Guimaraes E., Cruz Vieira L., Sivry Y., Zelano I., Montarges Pelletier E., Thil F. and Quantin C. (2015) Nickel isotope fractionation during tropical weathering of ultramafic rocks. *Chem. Geol.* **402**, 68 75.

Ratié G., Quantin C., Jouvin D., Garnier J., Calmels D., Ettler V., Sivry Y., Cruz Vieira L., Ponzevera E. and Garnier J. (2016) Nickel isotope fractionation during laterite Ni ore smelting and refining: Implications for tracing the sources of Ni in smelter affected soils. *Appl. Geochem.* **64**, 136 145.

Raudsepp M., Hawthorne F. C. and Turnock A. C. (1990) Crystal chemistry of synthetic pyroxenes on the join CaNiSi2O6 CaMgSi2O6 (diopside); a Rietveld structure refinement study. *Am. Mineral.* **75**, 1274 1281.

Regelous M., Elliott T. and Coath C. D. (2008) Nickel isotope heterogeneity in the early solar system. *Earth Planet. Sci. Lett.* **272**, 330 338.

Render J., Brennecka G. A., Wang S. J., Wasylenki L. E. and Kleine T. (2018) A distinct nucleosynthetic heritage for early solar system solids recorded by Ni isotope signature. *Astrophys. J.* **862: 28**, 18.

Richter F. M., Dauphas N. and Teng F. Z. (2009) Non traditional fractionation of non traditional isotopes: Evaporation, chem ical, diffusion and Soret diffusion. *Chem. Geol.* **258**, 92 103.

Roskosz M., Luais B., Watson H. C., Toplis M. J., Alexander C. M. O'D. and Mysen B. O. (2006) Experimental quantification of the fractionation of Fe isotopes during metal segregation from a silicate melt. *Earth Planet. Sci. Lett.* **248**, 851 867.

Roskosz M., Sio C. K. I., Dauphas N., Bi W., Tissot F. L. H., Hu M. Y., Zhao J. and Alp E. E. (2015) Spinel olivine pyroxene equilibrium iron isotopic fractionation and applications to natural peridotites. *Geochim. Cosmochim. Acta* **169**, 184 199.

Rouxel O., Dobbek N., Ludden J. and Fouquet Y. (2003) Iron isotope fractionation during oceanic crust alteration. *Chem. Geol.* **202**, 155 182.

Rugel G., Faestermann T., Knie K., Korschinek G., Poutivtsev M., Schumann D., Kivel N., Gunther Leopold I., Weinreich R. and Wohlmuther M. (2009) New measurement of the 60Fe half life. *Phys. Rev. Lett.* **14**, 103(7):072502. Epub 2009 Aug 14.

Sakai K., Laporte D., Vielzeuf D., Nakashima S. and Boivin P. (2003) Morphological analysis of olivine grains annealed in an iraon nickel matrix: experimental constraints on the origin of pallasites and on the thermal history of their parent bodies. *Meteorit. Planet. Sci.* **38**, 427 444.

Schauble E. A. (2004) Applying stable isotope fractionation theory to new systems. *Rev. Mineral. Geochem.* **55**, 65 111.

Schoenberg R. and von Blanckenburg F. (2006) Modes of planetary scale Fe isotope fractionation. *Earth Planet. Sci. Lett.* **252**, 342 359.

Scott E. R. D. (2007) Impact origin for pallasites. *Lunar and Planetary Science Conference* **1338**, 2284.

Shukolyukov A. and Lugmair G. W. (1993) Live iron 60 in the solar system. *Science* **259**, 1138 1142.

Solferino G. F. D. and Golabek G. J. (2018) Olivine grain growth in partially molten Fe Ni S: A proxy for the genesis of pallasite meteorites. *Earth Planet. Sci. Lett.* **504**, 38 52.

Solferino G. F. D., Golabek G. J., Nimmo F. and Schmidt M. W. (2015) Fast grain growth of olivine in liquid Fe S and the

formation of pallasites with rounded olivine grains. *Geochim. Cosmichica Acta* **162**, 259 275.

Steele R. C. J., Elliott T., Coath C. D. and Regelous M. (2011) Confirmation of mass independent Ni isotopic variability in iron meteorites. *Geochim. Cosmochica Acta* **75**, 7906 7925.

Tachibana S. and Huss G. R. (2003) The initial abundance of ^{60}Fe in the solar system. *Astrophys. J. Lett.* **588**, L41 L44.

Tang H. and Dauphas N. (2014) ^{60}Fe ^{60}Ni chronology of core formation in Mars. *Earth Planet. Sci. Lett.* **390**, 264 274.

Telus M., Huss G. R., Nagashima K., Ogliore R. C. and Tachibana S. (2018) In situ ^{60}Fe ^{60}Ni systematics of chondrules from unequilibrated ordinary chondrites. *Geochim. Cosmochim. Acta* **221**, 342 357.

Tsuchiyama A. and Fujimoto S. (1995) Evaporation experiments on metallic iron in vacuum. *Proc. NIPR Symp. Antarct. Meteorites* **8**, 205 213.

Tsunoda Y., Kurimoto Y., Seto M., Kitao S. and Yoda Y. (2002) Phonon density of states of gamma Fe precipitates in Cu. *Phys. Rev. B* **66**, 214304.

Wang, J., Davis, A.M., Clayton, R.N., and Mayeda, T.K. (1994). Kinetic isotopic fractionation during the evaporation of the iron oxide from liquid state. LPSCXXV, p.1459.

Wang X., Planavsky N. J., Reinhard C. T., Zou H., Ague J. J., Wu Y., Gill B. C., Schwarzenbach E. M. and Peucker Ehrenbrink B. (2016) Chromium isotope fractionation during subduction related metamorphism, black shale weathering, and hydrother mal alteration. *Chem. Geol.* **423**, 19 33.

Wasson J. T. and Choi B. G. (2003) Main group pallasites: chemical composition, relationship to IIIAP irons, and origin. *Geochim. Cosmochim. Acta* **67**, 3079 3096.

Watson H. C., Richter F., Liu A. and Huss G. R. (2016) Iron and nickel isotope fractionation by diffusion, with applications to iron meteorites. *Earth Planet. Sci. Lett.* **451**, 159 167.

Weyrauch M., Zipfel J. and Weyer S. (2019) Origin of metal from CB chondrites in an impact plume A combined study of Fe and Ni isotope composition and trace element abundance. *Geochim. Cosmochim. Acta* **246**, 123 137.

Young E. D., Galy A. and Nagahara H. (2002) Kinetics and equilibrium mass dependent isotope fractionation laws in nature and their geochemical and cosmochimical significance. *Geochim. Cosmochim. Acta* **66**, 1095 1104.

Zbiri M., Fennell T., Taylor J. W., Enderle M., Lau G. C., Cava R. J. and Johnson M. R. (2008) *Ab initio* lattice dynamics calculation of vibrational density of states and Raman active modes of the olivine mineral Ni_2SiO_4. *J. Phys.: Condensed Matter* **20**(285203), 7 pp.